PAPER • OPEN ACCESS

Assessment of validity of local neoclassical transport theory for studies of electric-field root-transitions in the W7-X stellarator

To cite this article: M.D. Kuczyński *et al* 2025 *Nucl. Fusion* **65** 016019

OPEN ACCESS
IOP Publishing | International Atomic Energy Agency
Nuclear Fusion
Nucl. Fusion **65** (2025) 016019 (21pp)
https://doi.org/10.1088/1741-4326/ad90f3

Assessment of validity of local neoclassical transport theory for studies of electric-field root-transitions in the W7-X stellarator

M.D. Kuczyński*, R. Kleiber, H.M. Smith, P. Helander, C.D. Beidler, M. Wappl, M. Borchardt, J. Geiger, S. Bozhenkov, A. Langenberg, T. Andreeva and the W7-X Team[a]

Max Planck Institute for Plasma Physics, Wendelsteinstrasse 1, Greifswald D-17491, Germany

E-mail: michal.kuczynski@ipp.mpg.de

Received 23 June 2024, revised 22 October 2024
Accepted for publication 11 November 2024
Published 20 November 2024

Abstract

The neoclassical ambipolarity condition governing the radial electric field in stellarators can have several solutions, and sudden transitions (in radius) between these can then take place. The radial position and structure of such a transition cannot be determined from local transport theory, and instead a non-rigorous model based on a diffusion equation for the electric field is usually employed for this purpose (Turkin *et al* 2011 *Phys. Plasmas* **18** 022505). We compare global (full plasma volume) drift-kinetic simulations of neoclassical transport in the Wendelstein 7-X stellarator with this model and find significant discrepancies. The position r_0 of the transition is not predicted correctly by the diffusion model, but the radial structure of the transition layer is in reasonable agreement if the diffusion coefficient is chosen appropriately. In particular, it should depend on the plasma temperature in the same way as the plateau-regime coefficient of neoclassical transport theory or the gyro-Bohm diffusion coefficient. In the small-gyroradius limit, the prediction of r_0 by the diffusion model simplifies to the so-called Maxwell construction (Shaing 1984 *Phys. Fluids* **27** 1567–9; Shaing 1984 *Phys. Fluids* **27** 1924–6). However, this property also emerges from a wide range of other mathematical models in the appropriate limit. The basic assumption underlying these models is that the diffusion, or generalisations thereof, is independent of the radial electric field, which is however unlikely to be the case in practice. Presumably this fact explains the discrepancy between the diffusion model and the drift-kinetic simulations. Finally, it is found that global simulations replicate the phenomenon of spontaneous root transitions driven by variations in the electron-to-ion temperature ratio, as predicted by local theory in the small-gyroradius limit.

[a] See Grulke *et al* 2024 (https://doi.org/10.1088/1741-4326/ad2f4d) for the W7-X Team.
* Author to whom any correspondence should be addressed.

Keywords: CERC, neoclassical theory, Monte Carlo PIC simulations, stellarator theory

(Some figures may appear in colour only in the online journal)

1. Introduction

Recent advancements in high-performance computing have significantly expanded the capabilities of computational plasma physics. Notably, in the area of magnetic confinement fusion, full-device simulations have become possible, which were previously limited by computational constraints. In stellarator research, gyrokinetic simulations can nowadays be carried out using global codes in which the computational domain includes the entire plasma volume rather than a single flux tube or a single flux surface. Global codes include GENE-3D [1], a continuum gyrokinetic code for turbulence simulations, FORTEC-3D [2], a particle-in-cell code for global neoclassical simulations, and EUTERPE [3], a particle-in-cell code capable of both global turbulence and neoclassical simulations.

Although global codes offer a more comprehensive description of plasma behaviour than local ones, their substantial computational costs still remain a significant limitation. Consequently, for specific applications, such as routine transport calculations for comparison with experimental data, reduced models are frequently preferred. However, employing these models necessitates a thorough understanding of their applicability limits. In the context of gyrokinetic simulations, this motivates the importance of comparing flux-tube, flux-surface, and global simulations, as conducted, for example, in studies of the ion-temperature-gradient (ITG) and trapped-electron-modes [4], as well as zonal flows [5].

Similarly, 'conventional' local neoclassical transport theory can be generalised by the inclusion of global effects. The local ansatz is adequate for calculating the neoclassical transport under most conditions, and has been used to great effect over the years. The Wendelstein 7-X (W7-X) stellarator was optimised for small neoclassical losses calculated in this way, and, indeed, a reduction in neoclassical energy transport was experimentally confirmed [6]. This accomplishment constitutes a significant milestone of local neoclassical theory.

Using numerical simulations two decades ago, it was verified that global effects are negligible for the low-collisionality neoclassical fluxes in W7-X [7]. This is because the temperature threshold, beyond which these effects become significant, is so high that it will not be reached under the typical operational conditions of the machine. However, under certain plasma conditions, the local ansatz can be violated, making global theory essential for a comprehensive description of plasma behaviour. One such situation, which is the central topic of this article, is the electron-to-ion root transition of the radial electric field E_r, characterised by the electric field changing from a positive to a negative value within a narrow radial region. This phenomenon has been experimentally observed in various stellarators [8] and also appears in tokamaks [9], though the physical origin of this phenomenon is different in this type of confinement devices [10]. The study of electron-to-ion root transitions is important for fusion research, since they can be favourable for confinement in future stellarator-type reactors. First, an electron root ($E_r > 0$) can be beneficial for expelling heavy impurities from the plasma core region. Secondly, the competing effects of the magnetic- and electric poloidal drifts can lead to large radial displacement of α-particles with reduced energy, which can be exploited for expelling helium ash in a stellarator-type reactor [11]. Furthermore, in the proximity of the transition location r_0 where $E_r = 0$, the strongly sheared $\boldsymbol{E} \times \boldsymbol{B}$ flow has the potential to suppress turbulence [12]. Due to the rapid spatial variations of E_r, in this scenario the local ordering is violated, and thus a global model is necessary. In particular, the question of accurately determining r_0 seems to lie outside of the scope of the local theory.

Nevertheless, a diffusion equation for the radial electric field that models nonlocal effects has been proposed, allowing an estimation of the transition point r_0 of the electric field [13, 14]. Despite early criticism [15–17], this model remains widely used for the verification of experimental data [18], as it usually produces a qualitative agreement between theory and experiment. In this article, we identify operational scenarios of W7-X where quantitative differences between the model electric field and the self-consistent, global neoclassical electric field are apparent. In particular, we analytically demonstrate that, in the limit of infinitely narrow transitions, a broad class of potential generalisations of the local theory all result in the same prediction for r_0, irrespective of the exact form of the diffusion coefficient assumed in this model. We then show numerically that a constant diffusion term cannot explain the large discrepancies observed between r_0 calculated with local and global simulations. Moreover, using global simulations, we verify a long-standing prediction of local neoclassical transport theory, i.e. the possibility of spontaneous transitions from ion to electron roots with a small variation in electron temperature at a given plasma radius [14]. Based on this analysis and studies of electron-root plasmas in the low electron-to-ion-temperature-ratio regime, we conclude that assuming a constant electric-field diffusion coefficient in the electric-field diffusion model is inappropriate for describing the transition region. To address this problem, we propose a radially dependent electric-field diffusion model that, in addition to resolving several issues encountered with the 'standard' model, accurately accounts for the dependence of the maximum of $|\frac{\mathrm{d}E_r}{\mathrm{d}r}|$ on the density and temperature plasma profiles for various configurations of W7-X. Our results do not, however, entirely eliminate the requirement for global simulations. In particular, for a given set of plasma density and temperature profiles and a magnetic configuration, the generalised diffusion model does not reliably predict the electric-field transition location found through global simulations with similar

parameters. Nevertheless, the model proves to be a computationally inexpensive tool for assessing the structure of the radial electric field in the W7-X stellarator, for instance, in the analysis of the impact of the sheared $\mathbf{E}\times\mathbf{B}$ flow on plasma turbulence, or for extrapolation of results obtained with global simulations. We note that this work builds on [19], which focused on the implementation of global neoclassical simulations in the gyrokinetic code EUTERPE. The following overview of the the local and global neoclassical transport models is intended to complement the review found therein.

2. Review of local neoclassical transport theory

2.1. The linearised drift-kinetic equation

In this work, we consider a single species plasma with ions indexed by i, and electrons by e. However, we will typically omit the species index for brevity, including it only when necessary. The distribution function of each species will be denoted by $f(t,\boldsymbol{R},H,\mu)$, where $\boldsymbol{R}$ is the gyrocentre position, $\mu = mv_\perp^2/2B$ the magnetic moment, and $H = mv^2/2 + Ze\Phi$ the energy. Here, Φ is the electric potential, e the elementary charge, Z the atomic number of the species, m their mass, and v the magnitude of the velocity vector with $v_\parallel$, $v_\perp$ its component parallel and perpendicular to the magnetic field $\boldsymbol{B}$. This results in the drift-kinetic equation

$$\frac{\partial f}{\partial t} + \left(\boldsymbol{v}_\parallel + \boldsymbol{v}_d\right)\cdot\frac{\partial f}{\partial \boldsymbol{R}} = C(f), \tag{1}$$

where $C(f)$ is a collision operator, whose form is given below. Furthermore, $\boldsymbol{v}_d = \boldsymbol{v}_{\boldsymbol{B}} + \boldsymbol{v}_\Phi$, with

$$\dot{\boldsymbol{R}} = \underbrace{v_\parallel \boldsymbol{b}}_{\boldsymbol{v}_\parallel} + \underbrace{\frac{m}{Ze}\frac{1}{B^*}\left[\mu \boldsymbol{b}\times\nabla B + v_\parallel^2 \boldsymbol{b}\times\kappa\right]}_{\boldsymbol{v}_{\boldsymbol{B}}} + \underbrace{\frac{1}{B^*}\boldsymbol{b}\times\nabla\Phi}_{\boldsymbol{v}_\Phi}, \quad \dot{H} = 0, \quad \dot{\mu} = 0, \tag{2}$$

where $B^* = B + \frac{m}{Ze}v_\parallel \boldsymbol{b}\cdot(\nabla\times\boldsymbol{b})$, and $\boldsymbol{b}\times\kappa = \frac{1}{B}[\boldsymbol{b}\times\nabla B + (\nabla\times\boldsymbol{B})_\perp]$. Depending on the ordering of the constituents in equation (1), expressions for transport in different magnetic configurations and collisionality regimes can be derived [20, 21, chapter 8.2]. Also, from a numerical perspective, solving equation (1) can be challenging because of the disparity between the timescales associated with the particles' motion along the magnetic field, their radial drift, and collisional scattering [22]. This problem can be addressed by expanding equation (1) around a local Maxwellian and linearising the resulting equation. Introducing the order parameter $\rho_* = \rho/L$, with ρ the largest Larmor radius (typically $\rho = \rho_i$) and $L \sim B/|\nabla B| \sim \Phi/|\nabla\Phi|$, the macroscopic scale of interest, for each species, the distribution function is written as

$$f = f_0 + \delta f, \tag{3}$$

$$f_0 = n\left(\frac{m}{2\pi T}\right)^{3/2}\exp\left(-\frac{H - Ze\Phi}{T}\right), \tag{4}$$

where the density $n(r)$, temperature $T(r)$, and $\Phi(r)$ are taken to be flux-functions, and $\delta f/f_0 \sim O(\rho_*)$. We use the radial coordinate $r = a\sqrt{s}$, with a the minor radius of the plasma edge, and $s\in[0,1]$ the normalised toroidal flux. The magnetic drift motion satisfies $v_{\boldsymbol{B}}/v_\parallel = O(\rho_*)$, and hence, under the assumption that δf varies on the length scale L, the following ordering estimate holds,

$$\boldsymbol{v}_{\boldsymbol{B}}\cdot\frac{\partial \delta f}{\partial \boldsymbol{R}} \Big/ \boldsymbol{v}_\parallel\cdot\frac{\partial f_0}{\partial \boldsymbol{R}} \sim O\left({\rho_*}^2\right). \tag{5}$$

Finally, the collision operator is linearised. In the simplest case, only its pitch-angle scattering part is considered, which takes the form

$$C(f) = \nu\mathcal{L}(f) = \nu\frac{1}{2}\frac{\partial}{\partial p}\left(1-p^2\right)\frac{\partial f}{\partial p}, \tag{6}$$

with $p = v_\parallel/v$ the pitch-angle variable, and ν the collision frequency, which is the sum of the inter- and intra-collision frequencies, given by [21, chapter 3.3]

$$\nu = \sum_\beta \nu_{\alpha/\beta}, \quad \nu_{\alpha/\beta} = \nu^0_{\alpha/\beta}\frac{\operatorname{erf}(x_\beta) - G(x_\beta)}{x_\alpha^3}. \tag{7}$$

Here, the normalised particle velocity is denoted by $x_\beta = v/v_{T\beta}$, where $v_{T\beta} = \sqrt{2T_\beta/m_\beta}$ is the thermal velocity of the species β, and a reference collision frequency $\nu^0_{\alpha/\beta}$ is written as

$$\nu^0_{\alpha/\beta} = \frac{n_\beta\left(Z_\alpha e\right)^2\left(Z_\beta e\right)^2\log(\Lambda)}{4\pi\,\epsilon_0^2 m_\alpha^2 v_{T\alpha}^3}, \tag{8}$$

where $\log(\Lambda)$ is the Coulomb logarithm, and ϵ_0 the vacuum permittivity. The error function $\operatorname{erf}(x)$ and the Chandrasekhar function $G(x)$ appearing in equation (7) have the definitions

$$\operatorname{erf}(x) = \frac{2}{\sqrt{\pi}}\int_0^x \exp\left(-t^2\right)\mathrm{d}t, \quad G(x) = \frac{\operatorname{erf}(x) - x\frac{\mathrm{d}}{\mathrm{d}x}\operatorname{erf}(x)}{2x^2}. \tag{9}$$

We note that ion-electron collisions effectively act as a small friction force on the ions [21, chapter 3.5], scaling as $\nu_{ii}\sqrt{m_e/m_i}$, and therefore will be disregarded throughout this article.

If the time derivative is assumed second order in ρ_* [21, chapter 6.5], this procedure results in the following linearised drift-kinetic equation,

$$\left(\boldsymbol{v}_\parallel + \boldsymbol{v}_\Phi\right)\cdot\frac{\partial \delta f}{\partial \boldsymbol{R}} - \nu\mathcal{L}(\delta f) = -\boldsymbol{v}_d\cdot\frac{\partial f_0}{\partial \boldsymbol{R}}, \tag{10}$$

where it should be noted that $\boldsymbol{v}_\Phi$ is tangential to flux surfaces since $\nabla\Phi = \Phi'(r)\nabla r$. From a numerical perspective, equation (10) has the significant advantage of being local and 'mono-energetic', that is r enters the equation as a mere parameter (i.e. no derivatives with respect to r are present), so that each flux surface can be treated independently, irrespective of the transport properties of other surfaces. Due to the simplified collision operator used, the same is true for the magnitude of the velocity v, which also enters only as a parameter.

A detailed discussion of various numerical techniques used to solve the linearised local drift-kinetic equation is given in [20]. In our work, local neoclassical simulations are performed using the code Neotransp, which utilises the mono-energetic diffusion coefficients data tabulated with DKES [22, 23] for the calculation of the radial electric field. In other words, using DKES, at each flux surface the mono-energetic transport coefficients are obtained by solving equation (10) for a fixed value of the electric-field. The reader is referred to [20] for more details regarding this calculation. Then, using Neotransp the value of the electric field at the considered flux surface is selected in accordance with the electric-field diffusion model to be introduced in the next section.

2.2. Ambipolarity condition and the electric-field diffusion model

The mono-energetic transport coefficient $D_{11}(r,\nu/v,E_r/vB)$ obtained with DKES depends on the minor radius (and consequently on the magnetic geometry), normalised collision frequency and the normalised electric field value only. Here, $E_r(r) = -\Phi'(r)$ is the local value of the electric field. In principle, for a selected magnetic equilibrium and for a choice of density and temperature profiles, the particle flux can be calculated for any desired value of E_r. For instance, for stellarators without a large Ohmic current, it follows that the total particle flux $\Gamma(E_r, r)$ across the considered flux surface is given by

$$\Gamma \equiv \left\langle \int \delta f \mathbf{v}_d \cdot \nabla r \mathrm{d}v^3 \right\rangle = -nL_{11}\left(\frac{n'}{n} - \frac{ZeE_r}{T} - \frac{3}{2}\frac{T'}{T}\right) - nL_{12}\frac{T'}{T}, \tag{11}$$

$$L_{1j} = \frac{2}{\sqrt{\pi}}\int_0^\infty K^{3/2-j}e^{-K}D_{11}(K)\,\mathrm{d}K, \tag{12}$$

where $\langle\cdot\rangle$ is the flux-surface average, primes represent differentiation with respect to r, the index j is equal to either 1 or 2, and $K = mv^2/(2T)$. In general it is also important to include the contribution of the inductive electric field to the particle flux (known as the Ware pinch [20]) in equation (11), which involves the mono-energetic coefficient D_{13}. For brevity, it is not written explicitly here, since the parallel electric field $\langle \mathbf{E}\cdot\mathbf{B}\rangle$ is zero.

To close the system with an equation for the electric field, we can apply the flux-surface average to the radial component of Ampère's law with the polarisation current retained, resulting in the following ambipolarity constraint on the particle flux,

$$\frac{\partial E_r}{\partial t} = \frac{e}{\epsilon}\left(\Gamma_e - Z_i\Gamma_i\right), \tag{13}$$

where we introduced ϵ, the neoclassical plasma permittivity.

$$\epsilon = \frac{m_p n_e}{B_{00}^2}\left(1 + \frac{b_{10}^2}{(r/R)^2\,\iota^2}\right), \tag{14}$$

with ι the rotational transform. B_{00} and $b_{10} = B_{10}/B_{00}$ are terms in the Boozer decomposition of $\mathbf{B}$ with b_{10} characterising the principal variation of $\mathbf{B}$ in the poloidal direction. It is worth noting that in the region where the electric field transition occurs, ϵ is approximately constant. In this case, ϵ can be interpreted as determining a time-scale for the evolution of the electric field, and thus in a stationary state its value is unmiportant. For simplicity, in Neotransp the above formula is evaluated at $r = a/2$, except for the electron density, whose value is taken at the magnetic axis. It is important to note that equation (13) holds even if most particle transport is caused by turbulence, because turbulent fluxes are inherently ambipolar to this order in ρ_* if governed by standard gyrokinetic theory [24–26]. In a steady state, we thus obtain

$$\Gamma_e = Z_i\Gamma_i. \tag{15}$$

It follows that, on each flux surface, the electric field can be calculated by finding the value E_r such that equation (15) is satisfied. (An exception occurs in axisymmetric and quasi-symmetric devices, where the ambipolarity condition is automatically satisfied.) When $E_r < 0$, the plasma is said to be in the ion-root, which is the usual situation in stellarators, particularly in an equithermal plasma, $T_e = T_i$, whereas $E_r > 0$ designates an electron-root, which can arise, for instance, when the electrons are significantly hotter than the ions, $T_e > T_i$.

However, this approach has limitations. In a typical stellarator experiment with strong ECRH heating in the core, the plasma exhibits an electron-root close to the centre while further out, where the ion and electron temperatures are comparable, the ion-root is instead present [27]. Hence, at some intermediate radius, E_r must transition between the two roots, crossing $E_r = 0$. Since this is typically a narrow transition, the ordering in equation (5) is violated. Instead,

$$\boldsymbol{v}_{\boldsymbol{B}}\cdot\frac{\partial \delta f}{\partial \boldsymbol{R}}\Big/\boldsymbol{v}_{\parallel}\cdot\frac{\partial f_0}{\partial \boldsymbol{R}} \sim O(\rho_*), \tag{16}$$

and thus, close to the transition region, nonlocal terms must be retained. When calculating the electric field in the framework of the local theory in these cases, this requirement is manifested by unphysical, multi-valued solutions of equation (15): an ion root E_r^i, an electron root E_r^e, and a third intermediate one, which is always unstable [28]. A widely adopted method for obtaining the electric field in the transition region is then to modify the ambipolarity equation, adding a diffusive term as follows [29],

$$\frac{\partial E_r}{\partial t} - \frac{1}{V'}\frac{\partial}{\partial r}DV'r\frac{\partial}{\partial r}\frac{E_r}{r} = \frac{e}{\epsilon}\left(\Gamma_e - Z_i\Gamma_i\right), \tag{17}$$

where $V'(r)$ is the derivative of the volume enclosed by the flux surface labeled by r, and D is the electric-field diffusion coefficient. Then, in a steady-state and in the limit of vanishingly narrow transition layer width (corresponding to $D \to 0^+$), this model results in a single-valued electric field. By calculating the following integral

$$\int_{E_r^i}^{E_r^e}(Z_i\Gamma_i - \Gamma_e)\,\mathrm{d}E_r \begin{cases} > 0 : \text{ion root } \left(E_r = E_r^i\right) \\ = 0 : \text{transition location} \\ < 0 : \text{electron root } \left(E_r = E_r^e\right) \end{cases}, \tag{18}$$

it is possible to determine which of the two solutions of equation (15) will be attained by the electric field in the transition layer. This criterion is called the Maxwell construction and results in an electric field characterised by a discontinuity located at the transition location r_*. However, for $D \neq 0$, the discontinuity is not present in the steady-state solutions of equation (17), but determining a suitable diffusion coefficient presents a significant issue, since it is unknown for general non-axisymmetric devices. In practical applications, it is usually treated as a free, constant parameter. This approximation already poses significant issues, since from a theoretical standpoint, D in the very least should depend on the particle gyroradius. In this case, it is unclear whether the Maxwell construction is recovered in the small-gyroradius-limit. As we shall see, it is possible to formulate diffusion equations, which violate the Maxwell construction, resulting in a different transition location of the electric-field than the one presented in equation (18). In the next section, we therefore analytically analyse various generalisations of equation (17) in the limit of vanishingly narrow transitions. In particular, we determine sufficient conditions for the Maxwell construction.

3. Maxwell construction for the electric field diffusion model

3.1. The standard case

To begin, consider the equation

$$D\frac{\mathrm{d}^2 E_r}{\mathrm{d}r^2} = J(E_r, r), \tag{19}$$

where $J(E_r, r) = (Z_i\Gamma_i(E_r, r) - \Gamma_e(E_r, r))\, e/\epsilon$. We now demonstrate that this equation, in the limit $D \to 0^+$, leads to the Maxwell construction (equation (18)).

As mentioned above, the ambipolarity equation (equation (15)) has one or three zeros as a function of E_r. We thus assume the existence of two points $r_{\min}$ and $r_{\max}$ such that for $r < r_{\min}$, the plasma is in the electron root, for $r > r_{\max}$ it is in the ion root, and $r_{\min} < r < r_{\max}$ is the region of multiple solutions, on which we now focus. Furthermore, $J > 0$ for a large positive electric field and $J < 0$ for a large negative electric field. We denote the corresponding smallest (largest) solution as E_r^i (E_r^e). Figure 1 shows a typical scenario as described above.

Let us first introduce a stretched coordinate $x \equiv (r - r_*)\sqrt{J_*/D_*}$, where r_* is the transition location, $\lambda_D = \sqrt{D_*/J_*}$ is a typical length scale of the diffusion process for characteristic values of the diffusion coefficient D_* and particle flux J_*. We are interested in the limit where $\lambda_D/r_* \to 0$, in which the transition region becomes very narrow, and thus introduce a small parameter $\epsilon = \lambda_D/r_* \ll 1$. We also write $x_{\min} = (r_{\min} - r_*)/\lambda_D$, and $x_{\max} = ((r_{\max}) - r_*)/\lambda_D$. With the convention $\tilde{D} = D/D_*$ (and accordingly for $\tilde{J}$), we obtain

$$\tilde{D}\frac{\mathrm{d}^2 E_r}{\mathrm{d}x^2} = \tilde{J}(E_r, x), \tag{20}$$

We impose the following boundary conditions,

$$E_r(x_{\min}) = E_r^e, \tag{21}$$

$$E_r(x_{\max}) = E_r^i, \tag{22}$$

and note that, somewhere in the interval $[x_{\min}, x_{\max}]$, E_r will 'jump' from E_r^e to E_r^i over a transition layer of width of order unity when measured in terms of the stretched coordinate x but of order ϵr_* in terms of the radius r. The location of this jump, i.e. where $x = 0$, can be found by noting that

$$\frac{\tilde{D}}{2}\frac{\mathrm{d}}{\mathrm{d}x}\left[\left(\frac{\mathrm{d}E_r}{\mathrm{d}x}\right)^2\right] = \tilde{J}(E_r, x)\frac{\mathrm{d}E_r}{\mathrm{d}x}, \tag{23}$$

which follows from multiplying equation (19) by $\frac{\mathrm{d}E_r}{\mathrm{d}x}$. We integrate this equation over an interval that is much wider than the transition region but much narrower than the minor radius, e.g. by computing

$$\int_{-\epsilon^\beta}^{\epsilon^\beta} \tilde{J}(E_r, x)\frac{\mathrm{d}E_r}{\mathrm{d}x}\mathrm{d}x = \frac{\tilde{D}}{2}\left(\frac{\mathrm{d}E_r}{\mathrm{d}x}\right)^2\Bigg|_{x=-\epsilon^\beta}^{x=\epsilon^\beta}, \tag{24}$$

where β is any constant between -1 and 0. The result becomes, in the limit $\epsilon \to 0$,

$$\int_{E_r^e(0)}^{E_r^i(0)} \tilde{J}(E_r, x)\,\mathrm{d}E_r = 0, \tag{25}$$

if $\tilde{D}$ does not vary on the short length scale of λ_D. Consequently, equation (19) satisfies the Maxwell construction. We provide a geometrical interpretation of this result in figure 1.

Furthermore, we observe that this procedure works equally well for any equation of the form

$$Df(r)\frac{\mathrm{d}}{\mathrm{d}r}\left(g(r)\frac{\mathrm{d}h(r)E_r}{\mathrm{d}r}\right) = J(E_r, r), \tag{26}$$

for smooth, positive functions $f(r)$, $g(r)$, and $h(r)$, in the limit $D \to 0$. With a change of variables, multiplication by $g(x)\frac{\mathrm{d}h(x)E_r}{\mathrm{d}x}/f(x)$, and integration across the transition region we obtain

$$\tilde{D}\int_{-\epsilon^\beta}^{\epsilon^\beta} \frac{\mathrm{d}h(x)E_r}{\mathrm{d}x} g(x)\frac{\mathrm{d}}{\mathrm{d}x}\left(g(x)\frac{\mathrm{d}h(x)E_r}{\mathrm{d}x}\right)\mathrm{d}x = \frac{\tilde{D}}{2}\int_{-\epsilon^\beta}^{\epsilon^\beta}\frac{\mathrm{d}}{\mathrm{d}x} \times \left[\left(g(x)\frac{\mathrm{d}h(x)E_r}{\mathrm{d}x}\right)^2\right]\mathrm{d}x \to 0, \tag{27}$$

in the limit $\epsilon \to 0$, and similarly,

$$\int_{-\epsilon^\beta}^{\epsilon^\beta} J(E_r, x)\frac{g(x)}{f(x)}\frac{\mathrm{d}h(x)E_r}{\mathrm{d}x}\mathrm{d}x = \int_{h(-\epsilon^\beta)}^{h(\epsilon^\beta)} J(E_r, x)\frac{g(x)}{f(x)}E_r\mathrm{d}h \tag{28}$$

$$+ \int_{E_r(-\epsilon^\beta)}^{E_r(\epsilon^\beta)} J(E_r, x)\frac{g(x)}{f(x)}h(x)\,\mathrm{d}E_r \to \frac{g(0)}{f(0)}h(0)\int_{E_r^e(0)}^{E_r^i(0)} J(E_r, x)\,\mathrm{d}E_r, \tag{29}$$

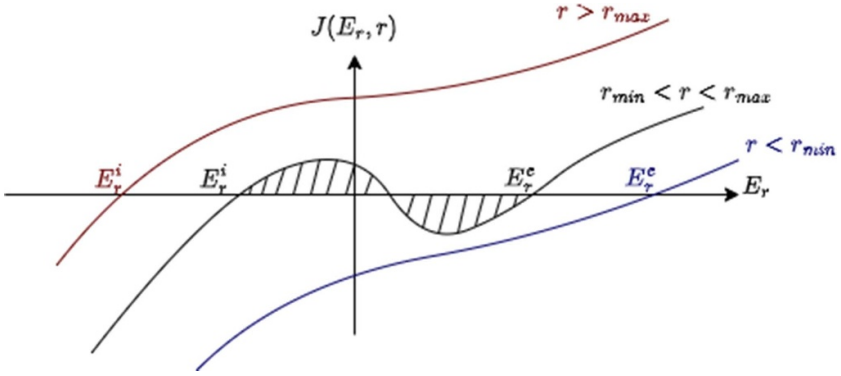

Figure 1. Illustration of the typical relationship between particle flux and radial electric field in stellarators. The red and blue lines correspond to the ion- and electron-root regimes, respectively, for which there is a unique value of the electric field satisfying the ambipolarity condition. The black line represents the region where multiple solutions occur. Depending on the area under this curve, for each radial location, either the ion- or electron-root solution is selected. Maxwell construction identifies the radial position r_*, at which this area is identically zero.

since $h(x)$ is continuous. As a corollary, in this limit, the stationary state of equation (17) satisfies the Maxwell construction, since we can identify $f(r) = -1/V'$, $g(r) = V'r$, and $h(r) = 1/r$.

3.2. Further generalisations

It is instructive to identify other generalisations of equation (15), for which the Maxwell construction holds. For instance, the argument provided in the previous section can also be applied for a fourth-order operator, i.e. for an equation,

$$D\frac{\mathrm{d}^4 E_r}{\mathrm{d}r^4} = J(E_r, r)\,, \tag{30}$$

since

$$\tilde{D}\int_{-\epsilon^\beta}^{\epsilon^\beta} E_r' E_r''''\mathrm{d}x = \tilde{D}\int_{-\epsilon^\beta}^{\epsilon^\beta}\frac{\mathrm{d}}{\mathrm{d}x}\left(E_r' E_r''' - \frac{E_r''^2}{2}\right)\mathrm{d}x \to 0. \tag{31}$$

Yet more generally, this approach is applicable to any sum of differential operators of even order,

$$\sum_n D_n \frac{\mathrm{d}^{2n} E_r}{\mathrm{d}r^{2n}} = J(E_r, r)\,, \tag{32}$$

which follows from an analogous calculation.

Further generalisation is also feasible. Consider, for instance, the integral operator

$$\tilde{D}_\epsilon[E_r] = \int_{-\epsilon^\beta}^{\epsilon^\beta} k(x - x')\, E_r(x')\,\mathrm{d}x', \tag{33}$$

where k is integrable and even, $k(y) = k(-y)$. Then,

$$\begin{aligned}\int_{-\epsilon^\beta}^{\epsilon^\beta}\frac{\mathrm{d}E_r}{\mathrm{d}x}\tilde{D}_\epsilon[E_r]\,\mathrm{d}x &= -\int_{-\epsilon^\beta}^{\epsilon^\beta} E_r\frac{\mathrm{d}\tilde{D}_\epsilon[E_r]}{\mathrm{d}x}\mathrm{d}x \\ &= \int_{-\epsilon^\beta}^{\epsilon^\beta}\int_{-\epsilon^\beta}^{\epsilon^\beta} E_r(x)\,k'(x - x')\,E_r(x')\,\mathrm{d}x\mathrm{d}x' = 0,\end{aligned} \tag{34}$$

since k' is odd. Thus, the solution to the equation $D_\epsilon[E_r] = J(E_r, r)$ satisfies the Maxwell construction in the limit $\epsilon \to 0$.

Even more generally, if D is any self-adjoint operator, i.e.

$$\int_{-\infty}^{\infty} f D[g]\,\mathrm{d}r = \int_{-\infty}^{\infty} g D[f]\,\mathrm{d}r, \tag{35}$$

we have

$$\begin{aligned}0 &= \int_{-\infty}^{\infty}\frac{\mathrm{d}}{\mathrm{d}x}\left(E_r\tilde{D}[E_r]\right)\mathrm{d}x = \int_{-\infty}^{\infty}\left(E_r'\tilde{D}[E_r] + E_r\tilde{D}[E_r']\right)\mathrm{d}x \\ &= 2\int_{-\infty}^{\infty} E_r' D[E_r]\,\mathrm{d}x,\end{aligned} \tag{36}$$

provided that $\frac{\mathrm{d}}{\mathrm{d}r}$ commutes with D.

These arguments show that the Maxwell construction works in a wide spectrum of cases, as long as the term that 'regularises' the transition is symmetric and linear in E_r. In the case of neoclassical transport, however, the assumption of linearity seems unlikely to be satisfied. If the usual contribution to the radial current from the local theory, $J(E_r, r)$, is nonlinear in E_r, why should the nonlocal one be linear? For example, if D depends on E_r and r in some known way but is independent of $E_r'(r)$, i.e. $D(E_r, r) = \epsilon F(E_r, r)$, equation (19) becomes

$$\epsilon\frac{\mathrm{d}^2 E_r}{\mathrm{d}r^2} = \frac{J(E_r, r)}{F(E_r, r)}, \tag{37}$$

and the transition occurs at the point where

$$\int_{E_r^i}^{E_r^e}\frac{J(E_r, r)}{F(E_r, r)}\mathrm{d}E_r = 0, \tag{38}$$

which is different from equation (18). Therefore, to determine the applicability of diffusion models such as equation (17), it

is necessary to compare the transition location r_* predicted by the Maxwell construction with the results of the global simulations.

Another intriguing aspect of the neoclassical theory in the small gyroradius limit is that, for a fixed radial location, the transition between the electron- and ion-roots due to variations in the electron temperature is expected to be spontaneous [13, 14]. This 'jump' is phenomenologically similar to the first-order phase transition between the liquid and gas phases of the ideal gas. It is a compelling question to determine whether this critical transition can also be reproduced by global simulations and how it compares with the corresponding prediction of the local, diffusive electric field model (equation (17)). However, as ρ_* decreases, the computational cost of global simulations increases, making simulations at small values of the normalised gyroradius impractical. Instead, we focus on comparing the predictions of local theory with global simulations using plasma profiles relevant for experiments in the W7-X stellarator rather than a larger device with smaller ρ_*.

Appendix provides a proof of the Maxwell construction found in the current literature, which is based on a variational formulation of equation (15). We note that our results extend this finding to a wide range of generalisations of the diffusion coefficient.

4. Self-consistent, global neoclassical transport simulations

4.1. Governing equations

Having discussed the calculation of the electric field in the framework of the local neoclassical theory and presented the derivation of the Maxwell construction, we now turn to the topic of self-consistent, global neoclassical transport equations. In our EUTERPE [3] global simulations, we solve the drift kinetic equation (equation (1)) for each species in coordinates $(\boldsymbol{R}, v_\parallel, \mu)$, so that

$$\frac{\partial f}{\partial t} + \left(\boldsymbol{v}_\parallel + \boldsymbol{v}_d\right) \cdot \frac{\partial f}{\partial \boldsymbol{R}} + \dot{v}_\parallel \frac{\partial f}{\partial v_\parallel} = C(f), \tag{39}$$

where the equation of motion for the energy (equation (2)) is replaced by

$$\dot{v}_\parallel = -\mu \nabla B \cdot \left[\boldsymbol{b} + \frac{m}{q}\frac{v_\parallel}{BB^*}\left(\nabla \times \boldsymbol{B}\right)_\perp\right] - \frac{q}{m}\left[\boldsymbol{b} + \frac{m}{q}\frac{v_\parallel}{B^*}\boldsymbol{b} \times \kappa\right] \cdot \nabla \Phi. \tag{40}$$

In these coordinates, the distribution function is written as

$$f = f_0 + \delta f, \quad f_0 = \frac{n_0}{\left(\sqrt{\pi} v_T\right)^3} e^{-\frac{v_\parallel^2 + v_\perp^2}{v_T^2}}, \tag{41}$$

with $n_0(r)$ the unperturbed density profile. However, we maintain the ordering given in equation (16), which restricts us from making any further simplifications. In the EUTERPE code, δf is allowed to be of arbitrary magnitude, but writing the distribution function this way has a numerical advantage for near-Maxwellian plasmas. We close the system self-consistently, calculating the electric potential by coupling the drift-kinetic equation to the gyrokinetic quasineutrality condition,

$$-\frac{m_i}{q_i}\nabla \cdot \left(\frac{n_{0,i}}{B^2}\nabla_\perp \Phi\right) = n_i - n_e, \tag{42}$$

where the perturbed density for each species is calculated by $n = \int f \mathrm{d}\mathbf{v}^3$. Equation (42) is supplemented by the following boundary conditions: $\Phi_{mn} = 0$ at the plasma boundary, and the natural regularity conditions at the magnetic axis, that is $\Phi'_{0n} = 0$, and $\Phi_{mn} = 0$, for $m \neq 0$ [3]. Thanks to the optimisation of W7-X, the $\Phi_{mn} \neq \Phi_{00}$ Fourier components are generally small in the absence of magnetic islands and plasma impurities. Thus, in this work we use a Fourier filter to simulate only the Φ_{00} component of the electric potential. Finally, the electric potential is initialised as $\Phi = 0$ at $t = 0$.

So far, no timescale separation has been imposed on the evolution of Φ, T_i, T_e and n profiles. However, provided that the relative changes in the n, T_i and T_e profiles which occur during the simulation are small, we can approximate $C(f)$ as the pitch-angle scattering operator (equation (6)). This is valid for global simulations of W7-X because its confinement is sufficiently optimised, so that energy scattering would have negligible influence on the results of global simulations [19].

We conclude this section with numerical aspects of the simulations: The simulation time is equal to one ion collision time of the ions in the core, which is on the order of 5×10^{-3} s. The time-step is set to a fixed value of $\Delta t = 0.5/\Omega_i$, where Ω_i is the ion gyrofrequency on the magnetic axis. The spatial grid is divided into $N_r = 32$ radial, $N_\theta = 16$ poloidal, and $N_\phi = 16$ toroidal points. The total number of markers is set to $N_e = 10^8$ for electrons and $N_i = 10^7$ for ions. Upon leaving the simulation domain, the markers are reinserted in a stellarator-symmetric way, whilst their weight is set to 0. This boundary condition represents a perfectly absorbing wall. Another possibility for the boundary conditions in EUTERPE is to keep the particles' weights unaltered during the reinsertion. However, we verified that for simulations in W7-X the choice between these two types of boundary conditions does not affect the steady-state solution for the radial electric field. This is because the particles are sufficiently well confined on the simulation timescale. Furthermore, periodic boundary conditions are employed in the toroidal direction, so that it is only necessary to simulate a single field period. A more detailed discussion of numerical aspects of the simulations is provided in [19, 30].

We remark that our approach is computationally intensive, typically requiring 10^5 CPU hours for standard simulations. In contrast, for the local theory, using precalculated mono-energetic transport coefficients from the DKES code, for a specific set of T_i, T_e, n profiles, Neotransp calculations of the electric field, whether using the Maxwell construction or the diffusion equation, can be completed in seconds for each plasma radius, on single-threaded applications.

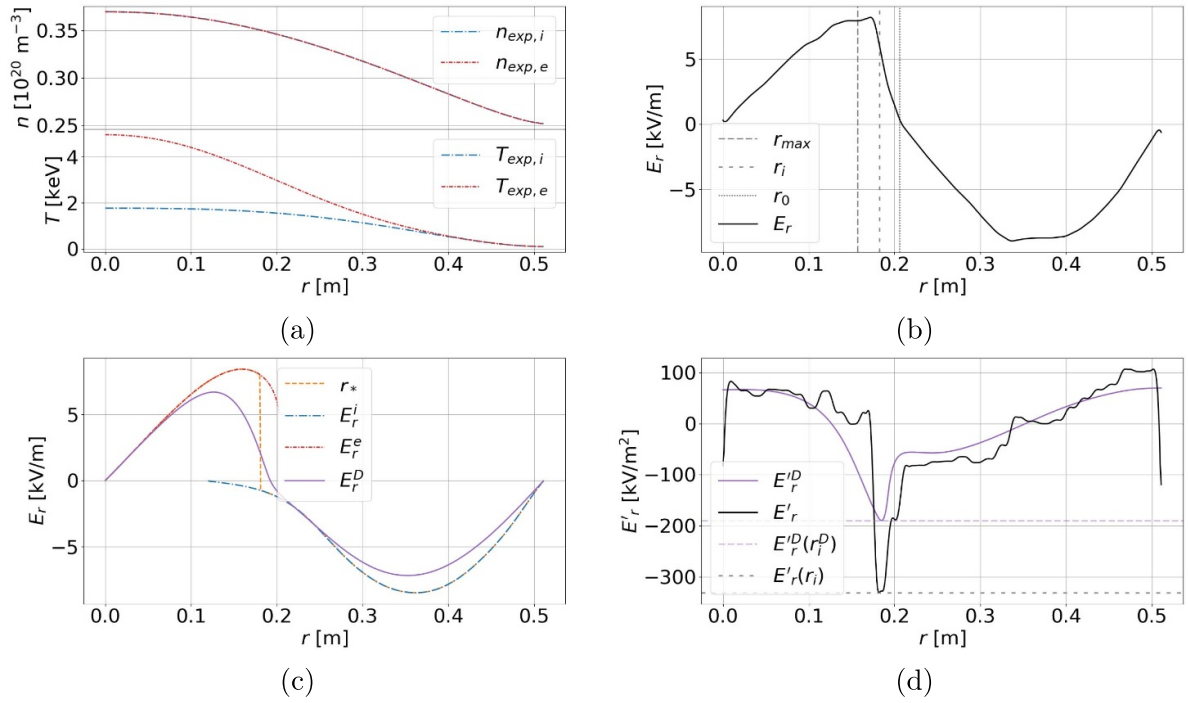

Figure 2. Quantities of interest for the benchmarking of local and global electric-field simulations. The simulated plasma profiles for both cases are shown in (*a*). The global electric field E_r, as well as its maximum $r_{\max}$, its inflection point r_i, and its zero r_0, are depicted in (*b*). The corresponding solution of the electric field diffusion model, E_r^D, with a demonstrative choice of the diffusion coefficient $D = 20\ \mathrm{m}^2\ \mathrm{s}^{-1}$ is presented in (*c*). Solutions associated with the limit $D \to 0$ are also included, that is the electron-root solution E_r^e, the ion-root solution E_r^i, and the transition location corresponding to the Maxwell construction r_*. Finally, a comparison of derivatives of E_r and E_r^D is shown in (*d*), with their minima indicated by the horizontal lines, accordingly.

4.2. Quantities of interest for the analysis of the results

From this point onward, for a specified set of profiles n, T_e, and T_i, and a chosen magnetic configuration, the global electric field simulated using EUTERPE is denoted by $E_r = -\Phi'(r)$. The local ion and electron root solutions, computed from the ambipolarity equation (equation (15)), are denoted by E_r^i and E_r^e, respectively. For a given value of D, the model electric field calculated from equation (17) is denoted by E_r^D. The transition location according to the Maxwell construction (equation (18)) is denoted by r_*, and is calculated by taking the limit $D \to 0$ of equation (17). This location can then be compared with the zero of E_r, represented by r_0, or with its inflection point, r_i. We further denote the location of the maximum of E_r as $r_{\max}$. For the electric field diffusion model, r_0^D, r_i^D, and $r_{\max}^D$ are defined accordingly. We also introduce the notion of submaximal transitions [19], for which the maximum of the global electric field occurs at a smaller radius than the maximum of the local electron root solution, i.e. $r_{\max} < r_{\max}^e$, with $r_{\max}^e$ the maximum of E_r^e. This distinction will be beneficial for the interpretation of our results. An empirical observation regarding the submaximal transitions is that the inflection point lies in the middle between the maximum and the zero of the electric field, $r_0 - r_i \approx r_i - r_{\max}$, so that $r_{\max}$ can be identified as the beginning of the transition, r_i as its centre and r_0 as its end. In contrast, for supramaximal transitions, i.e. when $r_{\max} = r_{\max}^e$, the maximum of the global electric field does not coincide with the beginning of the transition, and as a consequence, determining the width of the transition layer becomes challenging. Due to this difficulty, we avoid comparing the transition layer widths of the electric field calculated with the diffusion model and the global simulations in this work. Instead, we calculate and compare the minima of the radial derivatives of the electric fields, since they are defined unambiguously. Figure 2 visualises the quantities discussed above for local and global simulations in the standard configuration of the W7-X stellarator for interpolated experimental plasma profiles obtained from [31], further denoted as $n_{\mathrm{exp}} = n_{i,\mathrm{exp}} = n_{e,\mathrm{exp}}$, $T_{i,\mathrm{exp}}$, and $T_{e,\mathrm{exp}}$. These profiles are typical for electron root discharges obtained during W7-X operation phase 1.2b.

4.3. Profile parameterisation and the dimensionless plasma parameters

We wish to investigate the behaviour of the electric field based on the following, dimensionless plasma parameters; the ion collisionality, the normalised ion gyroradius, and the electron-to-ion temperature ratio,

$$\nu_i^* = \frac{a\nu_{\mathrm{th},i}}{v_{\mathrm{th},i}}, \quad \rho_i^* = \frac{v_{\mathrm{th},i}}{\Omega_i a}, \quad \tau = \frac{T_e}{T_i}, \tag{43}$$

where $\nu_{\mathrm{th},i} = \nu_{i/i}^0$ (see equation (8)), and $\Omega_i = ZeB/m_i$ is the ion gyrofrequency. Written in terms of plasma profiles, these expressions become

$$\nu_i^* = \frac{a\,(Ze)^4 \log(\Lambda)}{16\pi\,\epsilon_0^2}\frac{n}{T_i^2}, \quad \rho_i^* = \frac{\sqrt{2m_i}}{ZeBa}\sqrt{T_i}, \quad \tau = \frac{T_e}{T_i}. \tag{44}$$

We introduce a parameter α, scaling the n_{exp}, $T_{e,\mathrm{exp}}$, and $T_{i,\mathrm{exp}}$ profiles such that two of the three dimensionless plasma parameters are held constant, while the remaining one varies linearly with α:

- For ρ_i^*, $\alpha = \alpha_{\rho^*} \in \{0.75, 0.875, 1, 1.125, 1.25, 1.5\}$, and

$$T_e = \alpha_{\rho^*}^2 T_{\mathrm{exp},e}, \quad n = \alpha_{\rho^*}^4 n_{\mathrm{exp}}, \quad T_i = \alpha_{\rho^*}^2 T_{\mathrm{exp},i}. \tag{45}$$

- For ν_i^*, $\alpha = \alpha_{\nu^*} \in \{0.5, 1, 1.5, 2, 2.5, 3\}$, and

$$T_e = T_{\mathrm{exp},e}, \quad n = \alpha_{\nu^*} n_{\mathrm{exp}}, \quad T_i = T_{\mathrm{exp},i}. \tag{46}$$

- For τ, $\alpha = \alpha_\tau \in \{0, 0.5, 0.52, 0.54, 0.56, 0.58, 0.6, 0.7, 0.8, 0.9, 1, 1.5, 2, 2.5\}$, and

$$T_i = T_{\mathrm{exp},i}, \quad n = n_{\mathrm{exp}}, \quad T_e = \alpha_\tau\,(T_{\mathrm{exp},e} - T_{\mathrm{exp},i}) + T_{\mathrm{exp},i}. \tag{47}$$

  Note that this parameterisation ensures $T_i = T_e$ at the edge independently of α_τ, and that $\alpha_\tau = 0$ corresponds to an equithermal plasma.

These parameterisations will be our basic tool for the exploration of the solution space of the self-consistent, global neoclassical transport equations. For each of these simulations, we aim at comparing the earlier introduced quantities of interest between the global simulations and the corresponding predictions of the electric-field diffusion model based on local theory. First, in the subsequent section, we focus on the results concerning the Maxwell construction, i.e. the limit $D \to 0$ of equation (17).

5. Verification of the Maxwell construction

5.1. Comparison of the transition location

We begin by exploring the relationship between the transition location calculated using the Maxwell construction, with the zero, inflection point, and the location of the maximum of the global electric field, as a function of the dimensionless plasma parameters. Figure 3 illustrates the dependency of these four locations on the parameters α_τ, α_{ρ^*}, and α_{ν^*} introduced above. Focusing first on the global quantities, for the dependence on the ion-to-electron temperature ratio, we can distinguish three regions. For $\alpha_\tau < 0.58$ only the ion root solution is present, and consequently r_{max}, r_i, and r_0 are not depicted in figure 3(*c*) for this region. For each simulation, we compared the maxima of the local electron root and the global electric field and concluded that for $0.58 \leqslant \alpha_\tau \leqslant 1$, the transitions are submaximal and for $1.5 \leqslant \alpha_\tau$, they are supramaximal. Therefore, the change between the two types of transition occurs somewhere in the interval $1 < \alpha_\tau < 1.5$. For the dependence on the normalised ion gyroradius in figure 3(*a*), the transitions are submaximal for $\alpha_{\rho^*} \leqslant 1$ and supramaximal for $\alpha_{\rho^*} \geqslant 1.125$. For the dependence on ion collisionality in figure 3(*b*), the transitions are always submaximal. However, it is possible that this would not be the case if the calculation were repeated for higher values of collisionality, causing the transition to shift further inward, where the submaximal transitions tend to occur. Perhaps surprisingly, the transition type depends on the ion gyroradius in the global simulations, unlike the local calculations, which are very weakly dependent on the particle gyroradius.

Qualitatively, we can see that the zero and the inflection point of the global electric field follow a trend similar to that of the transition location according to the Maxwell construction for the ion-to-electron temperature ratio and ion collisionality parameterisations. The same is true for the dependence of the location of the maximum of the global electric field, especially when the transitions are submaximal. Altogether, this leads to the hypothesis that for high-τ plasmas, the variation of r_{max}, r_i, and r_0 with τ and ν_i^* coincides with the changes in r_*. This means that in a practical setting, if a transition location for certain plasma profiles is determined with a global simulation or measured experimentally, the transition location of the plasma with scaled τ and ν_i^* profiles can be determined by much faster, local simulations of r_*. On the other hand, the Maxwell construction does not provide a reliable prediction of the shift in the transition location with changing ion gyroradius.

This difficulty can be circumvented by referring to an analytical relation between the plasma parameters in the electron root regime. Based on the assumption that the electron roots are predominantly caused by the electron transport being in the $1/\nu$ regime, and the ion- in the $\sqrt{\nu}$ regime, the following expression has been derived [19]

$$\tau = C\mu_{i/e}^{1/7}\left(\frac{r}{a}\frac{\nu_i^*}{\epsilon_{\mathrm{eff}}\rho_i^*}\right)^{3/7}\left(\frac{b_{10}}{\epsilon_t}\right)^{4/7}, \tag{48}$$

where C is a constant, $\mu_{i/e}$ is the ion to electron mass ratio, ϵ_{eff} is the effective ripple, and $\epsilon_t = r/R$ with R the major radius. Provided that the constant C is determined from global simulations, this equation can be solved for the transition location estimate r_C, allowing an analysis of its dependence on the plasma parameters. Overall, for W7-X, r_* is a better indicator of the shifts in the transition location with changes in τ and ν_*^i for the high τ plasmas, however r_C outperforms the Maxwell construction when considering changes in ρ_*^i [19]. This finding suggests the most important factors in establishing an electron root, are the neoclassical flux of electrons in the $1/\nu$ regime, and that of ions in the $\sqrt{\nu}$ regime.

The results presented so far consider only the standard configuration of W7-X. We conclude this section by outlining simulation results for the experimental plasma temperature and density profiles in two additional magnetic configurations of the W7-X stellarator, namely the low- and high-mirror configurations [32]. Table 1 shows that in this case, the transition location according to the Maxwell construction is in quantitative disagreement with the zero and the inflection point of the electric field calculated with the global simulations, similar to what was found for r_C in our previous work. Thus, when

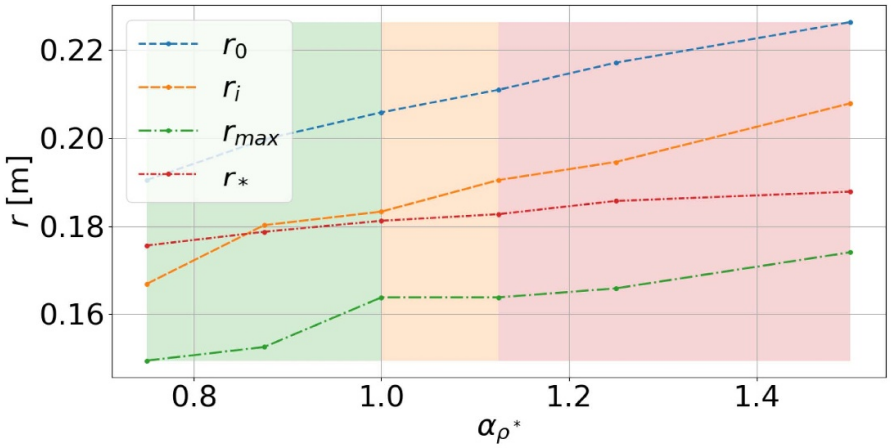

(a) ρ_i^* scaling

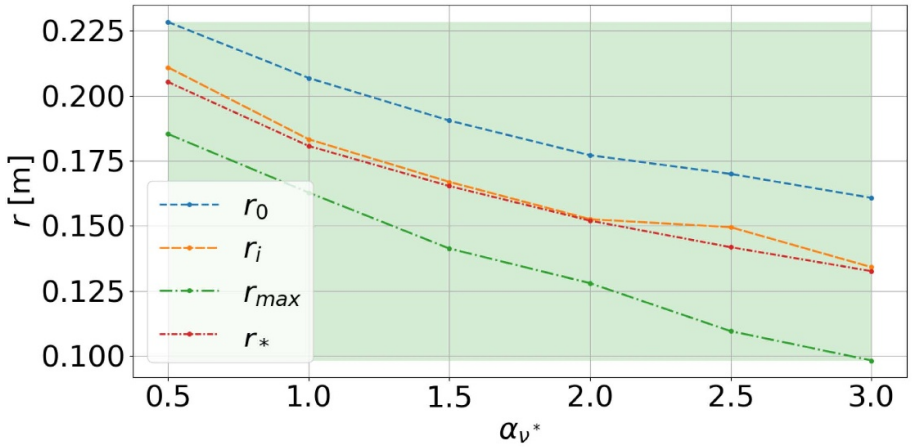

(b) ν_i^* scaling

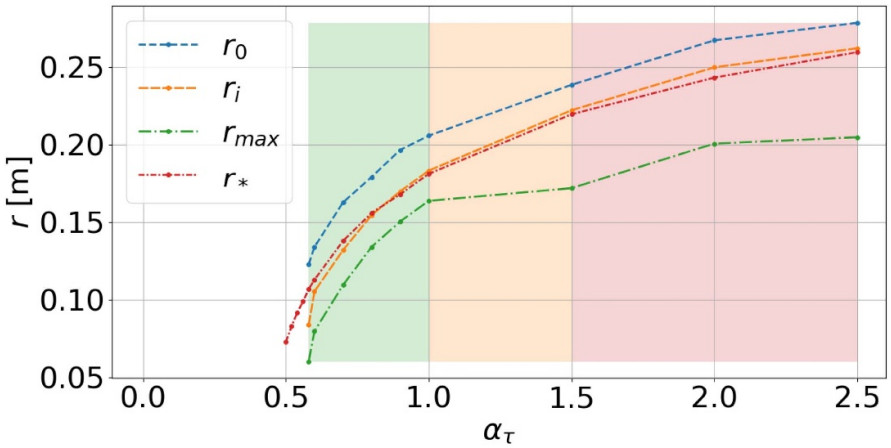

(c) τ scaling

Figure 3. Comparison of the transition location r_* according to Maxwell construction, with quantities $r_{\max}$, r_i, and r_0, calculated with global simulation, for ρ_*^i, ν_*^i and τ parameterisations. Results obtained for the plasma profiles $n_{\exp}$, $T_{i,\exp}$, and $T_{e,\exp}$ correspond to $\alpha_{\rho^*} = \alpha_{\nu^*} = \alpha_\tau = 1$, and are visible in each plot. The green (red) region indicates submaximal (supramaximal) transitions. The change in the two transition types occurs in the orange region. For the presented submaximal transitions, $r_{\max}$ can be interpreted as the beginning of the transition, r_i as the middle, and r_0 as the end.

considering changes in the magnetic geometry, both indicators of the transition location bear only a qualitative merit.

Two key questions follow from this analysis. First, is it possible to choose a suitable constant diffusion coefficient in the electric field diffusion equation, such that the resulting model captures the dependence of the transition location on the considered plasma parameters: ν_*^i, ρ_*^i, τ, and the magnetic configuration? Secondly, can this model allow for an accurate prediction of the absolute location of root transitions for arbitrary plasma profiles, without referring to comparisons with global simulations? In the next section, we endeavour to address these problems, beginning with analyses of the small τ regime included in our parameterisation.

5.2. Radial dependency of the electric-field diffusion coefficient and spontaneous root transition

We proceed with a comparison between the global simulations and the local diffusion model for the electron-to ion temperature ratio parameterisation. Our studies reveal that the discrepancy between the global and local predictions of the existence of the electron root for $0.42 \leqslant \alpha_\tau < 0.58$ can be mitigated by carefully choosing $D \neq 0$ in equation (17). Figure 4(c) shows that a value of $D = 20$ m^2 s^{-1} ensures that the electron root vanishes for $\alpha_\tau < 0.58$. However, comparing figures 4(c) and 3(c), we notice that for this choice of the diffusion coefficient, the location of the maximum and the zero of the electric field calculated with the local diffusion model differ significantly from their global counterparts. To understand what causes this disagreement, we first focus on the limit of $D \to 0$. In this case, the following equalities hold for submaximal transitions, $r_i^D = r_0^D = r_{\max}^D$ and for supramaximal transitions, $r_{\max}^D < r_i^D = r_0^D$. Then, in both cases, by increasing D, the relative positions of $r_{\max}^D$, r_i^D, and r_0^D are modified, typically leading to $r_{\max}^D \neq r_i^D \neq r_0^D$. However, it appears that this shift is not substantial enough to reproduce the relation $|r_{\max} - r_i| \approx |r_i - r_0|$ visible in figure 3(c) for the submaximal transitions. For supramaximal transitions, the discrepancy between the zero of the global electric field and the zero of the electric field calculated with the local diffusion model becomes smaller for large values of the electron-to-ion temperature ratio. However, for this choice of the diffusion coefficient, the disagreement between the location of the corresponding maxima persists for all α_τ. In fact, we found that the zero and the inflection point of the electric field calculated with the local diffusion model are insensitive to changes in the diffusion coefficient. In other words, varying it in general cannot solve the problem of the discrepancy of the location of the transition between local and global models. Trivially, it follows that it is not possible to choose a constant value of D, such that the electric field calculated with the local diffusion model and global simulations agree throughout the plasma volume. This is further supported by the fact that the electric-field diffusion model predicts submaximal transitions for $\alpha_\tau \in [0.58, 0.62]$, whereas for the global simulations, the submaximal transitions span the interval $\alpha_\tau \in [0.58, 1]$, possibly extending into the region $\alpha_\tau \in [1, 1.5]$.

Figure 4(a) also shows that the dependences on the normalised ion gyroradius of the inflection points of the electric field calculated with local diffusive model and global simulations are in disagreement for this choice of the electric field diffusion constant, which is an issue we had anticipated to be addressed by introducing $D \neq 0$ in equation (17). In fact, this discrepancy persists regardless of the choice of the constant D. Further, table 1 shows the comparison of the radial location of interest between global and local simulations for the experimental profiles across different magnetic configurations of W7-X. We notice a discrepancy of the order of the transition layer width between these locations for the low- and high-mirror configurations. Consequently, the constant diffusion coefficient model, while improving on the results of the Maxwell construction and the analytical scaling law presented in the previous section, does not capture the full complexity of the electric-field root transitions.

The Maxwell construction can also incorrectly describe the electric-field root transitions. To demonstrate this, we now return to the limit $D \to 0$ of the local theory, addressing the question of the existence of spontaneous root transitions of the radial electric field with small variations in the electron-to-ion temperature ratio as predicted by the local theory. We compare how the global and local diffusive model electric fields depend on the electron-to-ion temperature ratio for two selected radii, $r = 6$ cm and $r = 18$ cm. Figure 5(a) shows that for $r = 6$ cm, the electric field spontaneously transitions from the ion- to electron-root solution in both global simulation and in the limit of $D \to 0$ of local simulations. Nevertheless, there is a discrepancy between the critical value of α_τ at which this transition occurs, since the local code predicts a transition at a slightly lower value of $\alpha_\tau \approx 0.49$ compared to the global prediction of $\alpha_\tau \approx 0.52$. For $r = 18$ cm, we see that the transition to the electron root is gradual in the global case, as opposed to the local calculation, for which the transition is always spontaneous. This shows that close to the plasma core, the electric field can spontaneously transition between the ion- and electron-roots under small perturbations in the electron-to-ion temperature ratio.

It is currently unclear whether the initial condition for Φ at $t = 0$ influences the stationary solution of global simulations. In this study, we use the most common initial conditions for each code: $\Phi = 0$ for the global EUTERPE simulations, and the electric field calculated according to the Maxwell construction for the local, diffusive model simulations in Neotransp. The observed disagreement of the existence of electron roots in the low τ regime could potentially be attributed to these differing initial conditions, though we do not expect the initial conditions to impact the stationary state for a sufficiently large τ. This is also the reason why no hysteresis cycle is visible in figure 5. In a further study the existence of hysteresis in these models will be investigated.

Figures 5(c) and (d) show that by introducing $D \neq 0$ into the electric field diffusion equation, it is possible to improve on the solution of the ambipolarity equation. In particular, for $D \approx 6$ m^2 s^{-1}, both the global and local solutions align well for $r = 6$ cm. However, for $r = 18$ cm, we see that this value of D does not provide an agreement between the global and local codes. A suitable value of D for this radius, which matches the electric field between the local and global solutions, is found

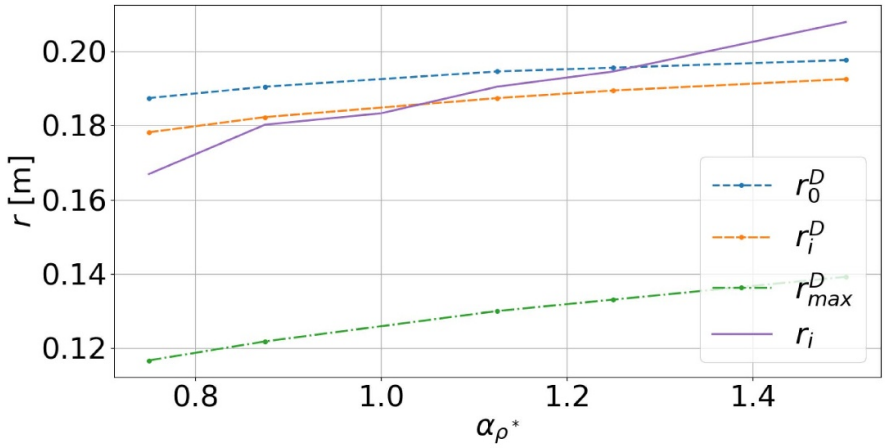

(a) ρ_i^* scaling

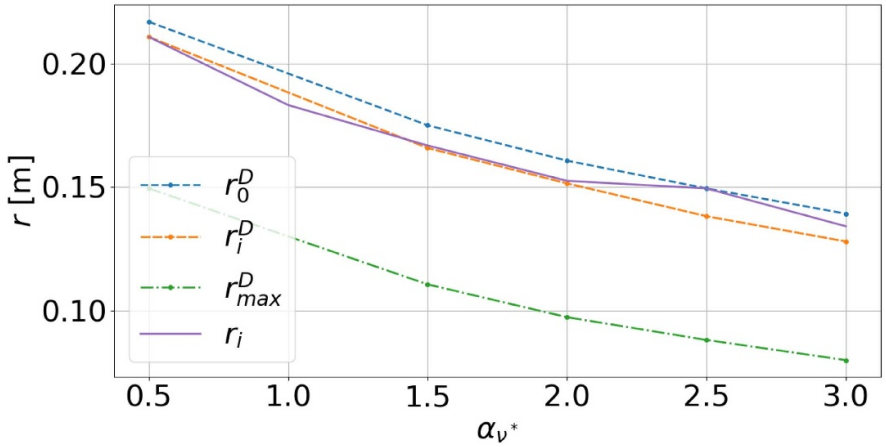

(b) ν_i^* scaling

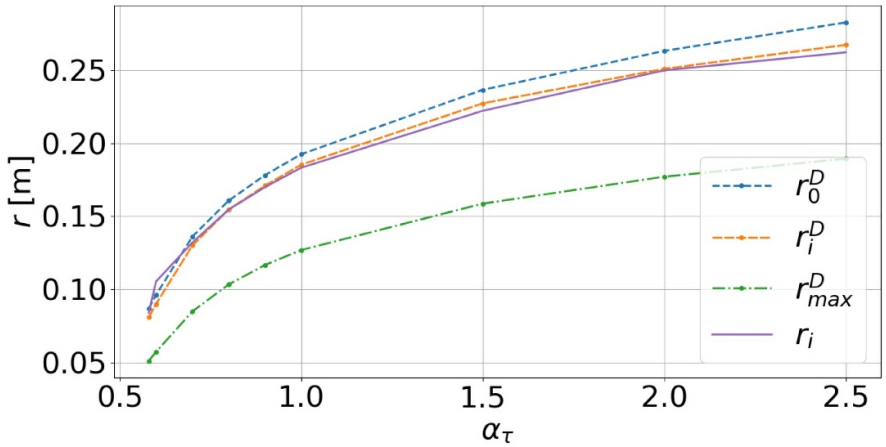

(c) τ scaling

Figure 4. Dependence of r_0^D, r_i^D, and $r_{\max}^D$ on α for ρ_*^i, ν_*^i and τ parameterisation, for $D = 20$ m^2 s^{-1} in the constant diffusion coefficient model. The purple line corresponds to r_i calculated with global simulations. The lines representing the remaining positions, r_0 and $r_{\max}$ are illustrated in figure 3 and have been omitted for a clearer presentation.

to be $D \approx 2$ m^2 s^{-1}. This suggests that the electric field diffusion coefficient decreases with r. This observation aligns with the findings of the previous paragraph, wherein a value of $D = 20$ m^2 s^{-1} was necessary to 'suppress' local electron-root solutions for $\alpha_\tau < 0.58$, which occur in close proximity to the magnetic axis. Additionally, for this value of the diffusion coefficient, figure 2(c) shows a significant difference between the electric field calculated with the diffusion equation and

Table 1. Comparison of the location of the maximum of the electric field $r_{\max}$, its inflection point r_i, its zero r_0 and transition location according to Maxwell construction r_* for different magnetic configurations of W7-X (all in cm). Results for local simulations with a diffusion coefficient value of $D = 20$ m^2 s^{-1} are also shown.

Configuration	$r_{\max}$	r_i	r_0	r_*	$r^D_{\max}$	r^D_i	r^D_0
High-mirror	23.7	26.3	27.9	24.2	18.2	25.1	25.5
Low-mirror	18.9	21.1	23.1	19.0	13.6	18.4	19.0
Standard	16.4	18.3	20.6	18.2	12.7	18.5	19.2

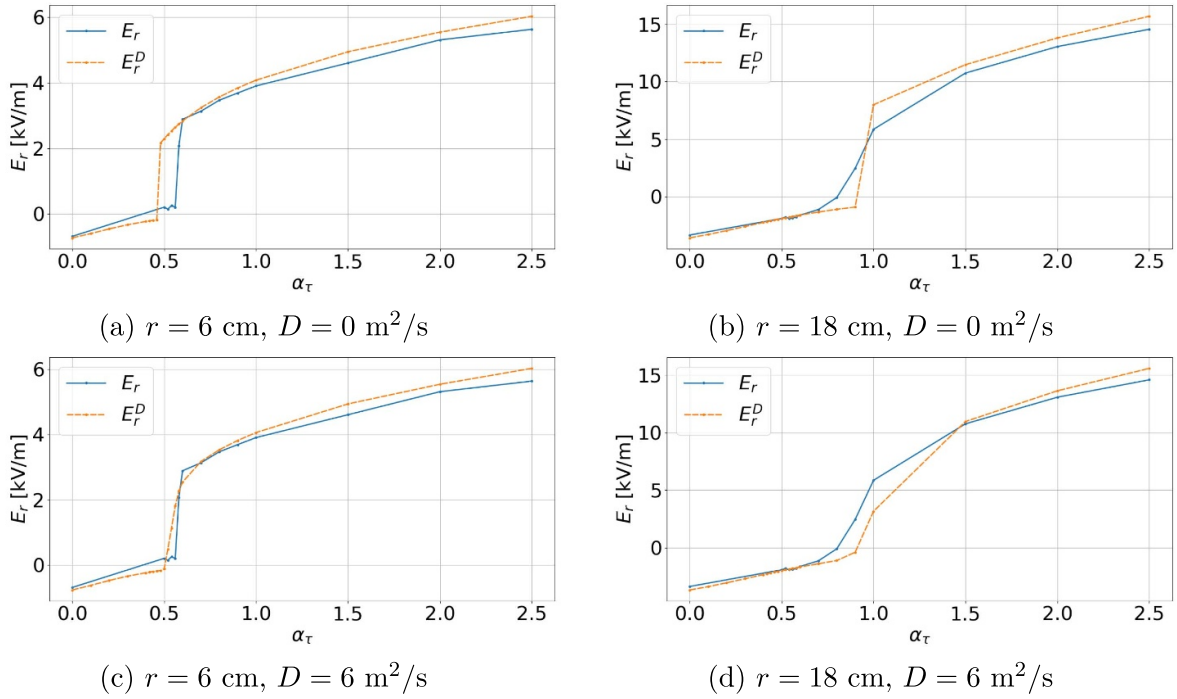

(a) $r = 6$ cm, $D = 0$ m^2/s (b) $r = 18$ cm, $D = 0$ m^2/s

(c) $r = 6$ cm, $D = 6$ m^2/s (d) $r = 18$ cm, $D = 6$ m^2/s

Figure 5. The relationship between E_r and α_τ for $r = 6$ cm (left) and $r = 18$ cm (right). The blue lines represent global solutions, while the orange lines represent local solutions. Local solutions are associated with $D = 0$ m^2 s^{-1} (top) and $D = 6$ m^2 s^{-1} (bottom). Notably, the root-transition is not spontaneous for the global calculation at $r = 18$ cm, since the electron-root exists already at $\alpha_\tau = 0.9$.

the 'pure' ion-root solution, which is not an expected result, since the local neoclassical ordering (equation (5)) is applicable in this regime, which in turn necessitates $D \approx 0$ m^2 s^{-1}. As a consequence of these findings, it is natural to consider a generalisation of the electric field diffusion equation, where $D(r)$ is a function of radius. However, rather than estimating this dependency directly, from a physical perspective, for a chosen magnetic configuration, it is much more instructive to study the dependence of the diffusion coefficient on the plasma parameters, i.e. $D(\tau, \rho_i^*, \nu_i^*)$. Such a representation of the diffusion coefficient is admissible for equation (17) [33]. This is the problem addressed in the next section.

6. Generalisation of the electric-field diffusion equation

6.1. Proposed metric for comparison of global and local calculations

Before proposing a generalisation of equation (17), we shall quantify the differences between the global electric field and that calculated with the local diffusion model, for various values of the diffusion coefficient and plasma parameters: ν_i^*, ρ_i^*, and τ. We propose the following metric

$$d \equiv \left| E_r'(r_i) - E_r'^D\left(r_i^D\right) \right|. \tag{49}$$

We note that $\lim_{D\to\infty} E_r'^D\left(r_i^D\right) = 0$, and that $\lim_{D\to 0} E_r'^D\left(r_i^D\right)$ diverges. In addition, $E_r'^D\left(r_i^D\right)$ is a monotonic function of D, so that for any choice of plasma profiles and magnetic configuration, the metric d is optimised for a unique D. From a practical point of view, $E_r'^D\left(r_i^D\right)$ is related to the $\mathbf{E}\times\mathbf{B}$ shearing rate, which has the potential to suppress microturbulence, such as ITGs. Determining this shearing rate without resorting to global simulations is the objective of the analysis in this section.

Figure 6 shows the dependence of d on D and α, for the ρ_i^*, ν_i^*, and τ parameterisations. For the dependence on the normalised ion gyroradius, visible in figure 6(*a*), we observe that there is a strong, positive correlation between the optimal value of D and α_{ρ^*}. An intuitive interpretation of this observation is that the importance of nonlocal effects scales positively with the magnitude of ρ_i^*. For the dependence on ion

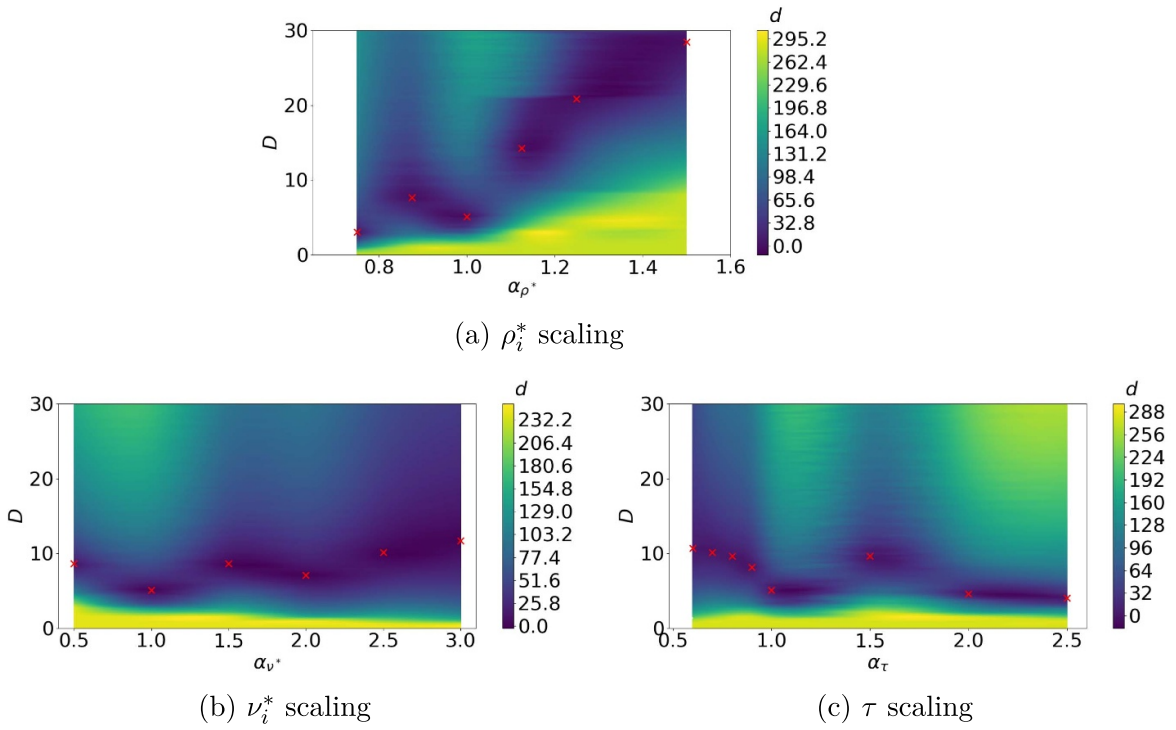

Figure 6. Dependence of the metric d on D and α for the ρ_i^*, ν_i^* and τ parameterisations for the constant diffusion coefficient electric field model. For each α, the black crosses indicate where $d=0$, from which the optimal value of D is obtained.

collisionality, shown in figure 6(*b*), we notice that there is no significant variation of the optimal value of D on α_{ν^*}. An analogous observation holds for the supramaximal transitions in the electron-to-ion temperature ratio parameterisation, indicated in figure 6(*c*). Finally, for the submaximal transitions in the latter parameterisation, we observe that there is a negative trend with increasing α_τ. Since these transitions typically occur close to the magnetic axis, this aligns with the earlier finding that the diffusion coefficient is a decreasing function of the radius. Overall, the most significant variation in the optimal diffusion coefficient is found for the dependence on the normalised ion gyroradius.

Finally, we note that alternative metrics, such as $|r_0 - r_0^D|$, or $|r_i - r_i^D|$ may not be appropriate for this analysis, since these measures are insensitive to variations in D, as indicated in section 5.2. In fact, further investigation has shown that these metrics are typically optimised for a wide range of D, for instance $D \in (5, 30)$ m^2 s^{-1}. We are thus in a position to propose a model with which we attempt to minimise the metric d by incorporating the strong dependece of the electric field diffusion coefficient on the particle gyroradius.

6.2. Generalised diffusion equation for the electric field

A straightforward and conceptually appealing approach is to relate the electric field diffusion coefficient to the neoclassical particle diffusion coefficient L_{11}. According to the scalings associated with the $1/\nu$, $\sqrt{\nu}$, plateau and Pfirsch-Schlüter collisionality regimes, the plateau regime has the desired property that the diffusion coefficient varies inversely with the magnetic field (and consequently with ρ_i^*) and is independent of ν_*^i. Therefore, we propose the following generalisation of the electric field diffusion equation:

$$\frac{\partial E_r}{\partial t} - \frac{1}{V'}\frac{\partial}{\partial r}\zeta L_{11}^{\mathrm{p}} V' r \frac{\partial}{\partial r}\frac{E_r}{r} = \frac{e}{\epsilon}\left(\Gamma_e - Z_i\Gamma_i\right), \tag{50}$$

where the constant ζ is to be determined from global simulations, and

$$L_{11}^{\mathrm{p}} = \left(\frac{\pi}{2}\right)^{1/2} \frac{G}{R\iota}\left(\frac{T}{qB}\right)^{3/2}\left(\frac{m}{qB}\right)^{1/2} \tag{51}$$

is the particle diffusion coefficient L_{11}^{p} for the plateau regime, where q is the particle charge, and G a geometry-dependent factor. For the W7-X stellarator, the following approximation can be applied,

$$G = \left(b_{10}\frac{R}{r}\right)^2. \tag{52}$$

Figure 7 illustrates L_{11}^{p} calculated for the plasma profiles $T_{i,\mathrm{exp}}$, $T_{e,\mathrm{exp}}$, and n_{exp} in the W7-X standard configuration. We notice that L_{11}^{p} decreases with r except in the vicinity of the magnetic axis.

To find the optimal value of ζ, we minimised the metric d, analogously to what was done earlier for the case of the constant diffusion coefficient electric field model. The value of d was calculated by taking $d \equiv \left|E_r'(r_i) - E'\zeta_r\left(r_i^{\zeta}\right)\right|$, where the index ζ refers to the quantities of interest calculated for the

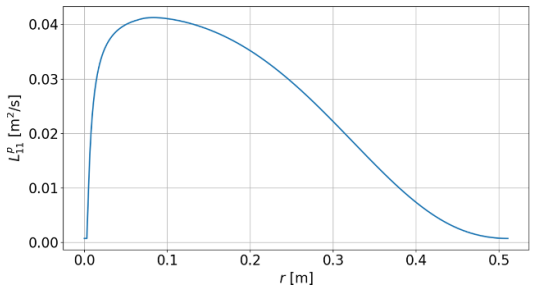

Figure 7. Radial dependency of L_{11}^p for the plasma profiles $T_{i,\mathrm{exp}}, T_{e,\mathrm{exp}}$, and n_{exp} in the standard configuration of W7-X.

generalised electric field diffusion model, the electric field E_r^ζ, its inflection point r_i^ζ, zero r_0^ζ, and the location of the maximum r_{max}^ζ. The resulting dependence of d on ζ and parameters α_τ, α_{ρ^*}, and α_{ν^*} is illustrated in figure 8. For the ion collisionality and electron-to-ion temperature ratio dependencies, visible in figures 8(b) and (c), the observed trends are similar to those corresponding to the constant diffusion coefficient seen in figures 6(b) and (c). However, for the normalised ion gyroradius dependence shown in figure 8(a), we observe that ζ is not correlated with α_{ρ^*}, which is different from the dependence of D on α_ρ^* seen in 6(a). This suggests that the model proposed in equation (50) correctly reproduces the dependence of the global $E_r'(r_i)$ on ρ_i^*, ν_i^*, and τ. The obtained value $\zeta = 240$ shows that the diffusion coefficient of the electric field is significantly larger than the diffusion coefficient of particles in the plateau regime, on which we based our fit. Figure 9 shows the comparison between the local electric field E_r^ζ calculated with the generalised diffusion equation for this value of ζ and the global E_r for the profiles $T_{i,\mathrm{exp}}$, $T_{e,\mathrm{exp}}$, and n_{exp} in the W7-X standard configuration. We observe that the slope of the electric fields in the transition region are in qualitative agreement. Furthermore, due to the radial dependency of L_{11}^p, for large r, E_r^ζ does not depart significantly from the ion root solution, in contrast to what is visible in figure 2(c) for the constant diffusion coefficient model. Nevertheless, for this simulation, we observe that the transition region of E_r^ζ is shifted inward with respect to the global E_r.

We now analyse the dependence of the locations of interest of the electric field calculated with the generalised diffusion equation on the dimensionless plasma parameters. Figure 10 shows these results, the interpretation of which is similar to what was established above for the constant diffusion coefficient electric field model. That is, the existence of electron roots is correctly characterised in the low electron-to-ion temperature ratio regime. The trend of the inflection points of global and local calculations align for both, ν_i^* and τ parameterisations, but not for the ρ_i^* parameterisation. In all cases, the curves of the maxima and the zeros do not align between the two models. For the inflection point, we noted earlier that r_i^D is not susceptible to changes in D for the constant diffusion coefficient electric field ambipolarity equation. This property is also reproduced for the variations of ζ in the now radially dependent diffusion coefficient. Therefore, the analytical results of section 3 suggest that the transition location will be close to the location predicted by the Maxwell construction for both models, irrespectively of the chosen values of D and ζ. To circumvent this issue, it is thus necessary to modify equation (17), for instance, by allowing the diffusion coefficient to depend on the electric field (see equation (38)).

We conclude this section with a comparison of quantities of interest between global simulations and the local, radially dependent diffusion-coefficient model for different magnetic configurations of W7-X. Table 2 summarises this information for the simulations with the experimental plasma profiles $T_{i,\mathrm{exp}}$, $T_{e,\mathrm{exp}}$, and n_{exp}. It is observed that there was no clear improvement compared to the constant-diffusion-coefficient model for various indicators of the transition location. We also notice that $E_r'(r_i)$ and $E'\zeta_r\left(r_i^\zeta\right)$ are in qualitative agreement, with the observed relative differences of the same order as for fitted data.

The arguments provided in this section have shown that the generalised diffusion equation model for the calculation of the electric field has the advantage over the commonly implemented constant diffusion coefficient model in that it is able to correctly account for the maximum of the derivative the electric field. However, as mentioned earlier, the discrepancies between the transition location can be in general large. Nevertheless, for many discharges in W7-X, the transition location agrees qualitatively with the local theory. In the next section, we show that in such cases the generalised diffusion equation model can be utilised to estimate the importance of the radially sheared poloidal plasma flow on the turbulence suppression.

7. Possible suppression of turbulence in the transition region

The results of the preceding section encourage an investigation of the applicability of the radially-dependent diffusion-coefficient model for W7-X discharges, which were not included in the fitting procedure of the parameter ζ described in the earlier section. Before delving into this comparison, we estimate the width of the region over which turbulence is expected to be reduced thanks to the shear of the $\mathbf{E}\times\mathbf{B}$ flow.

The growth rate γ of the ITG instability can be approximated as follows [34, 35],

$$\gamma \approx \varsigma \frac{v_{T_i}}{L_T}, \tag{53}$$

where $L_T = T_i/|\nabla T_i|$ is the characteristic length scale associated with the ion temperature gradient. We use a representative value of the constant $\varsigma = 0.05$, which was determined by linear, electrostatic, gyrokinetic simulations of growth rates in the W7-X high-mirror configuration, for the radial location $r/a = 0.7$, where the fluctuations are the strongest [36]. We employ the well-known Waltz criterion for the condition of the suppression of ITG growth rates due to the strongly sheared

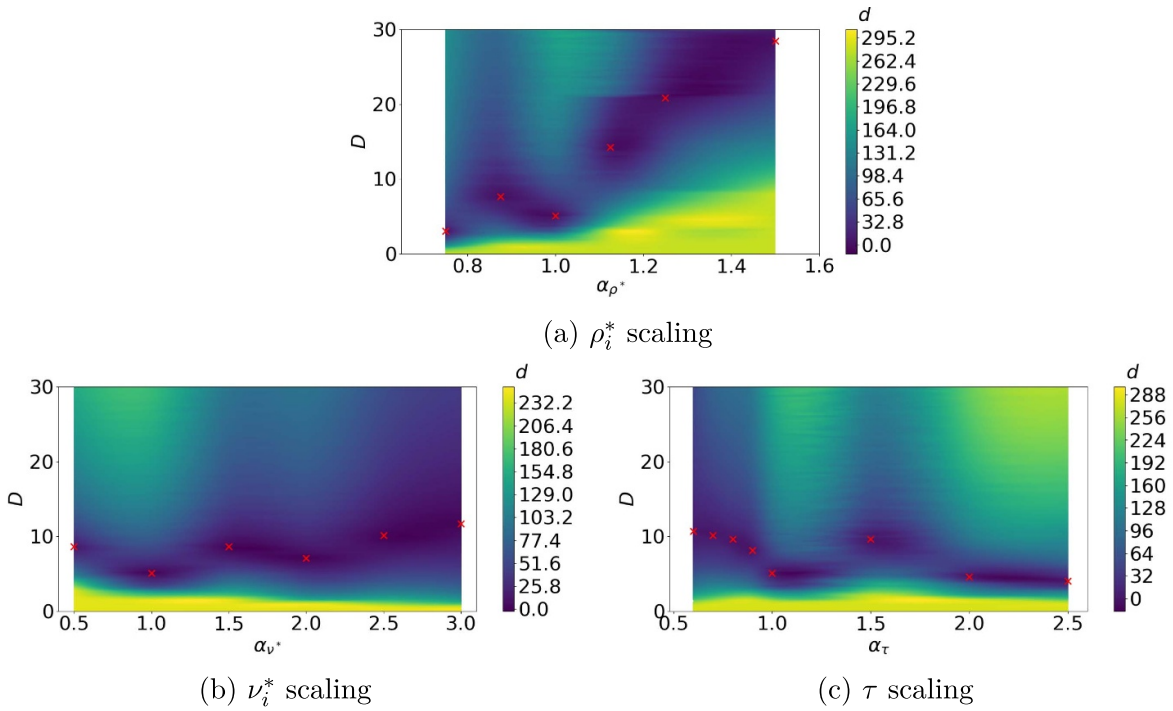

Figure 8. Dependence of the metric d on ζ and α for the ρ_i^*, ν_i^* and τ parameterisations for the proposed, radially-dependent diffusion coefficient model. For every α, the black crosses show where $d = 0$, corresponding to the optimal value of ζ.

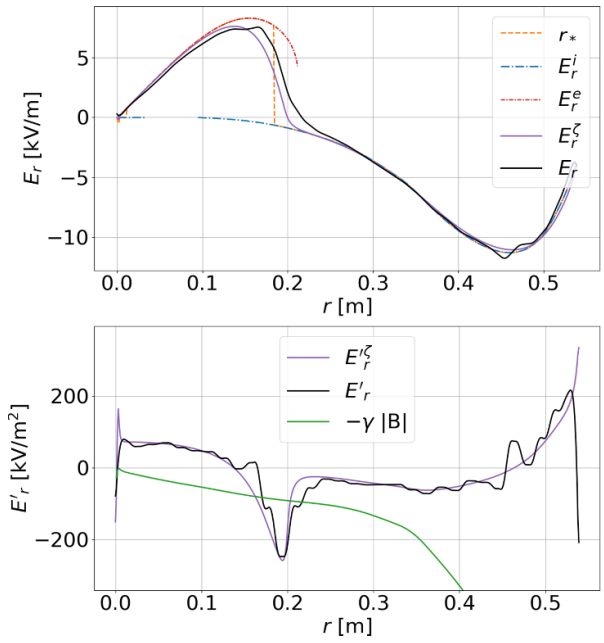

Figure 9. Radial electric field and its derivative calculated with global simulations and local, radially dependent diffusion coefficient models with $\zeta = 240$ for the plasma profiles $T_{i,\mathrm{exp}}$, $T_{e,\mathrm{exp}}$ and n_{exp} depicted in figure 2(*a*). The electric field plot also shows the ion- and electron-root solutions and the transition location according to Maxwell construction.

$\mathbf{E} \times \mathbf{B}$ flow in the transition region as follows [37, 38]

$$\left| \frac{E_r'}{B} \right| > \gamma. \tag{54}$$

Turbulence is then expected to be suppressed in the region where this inequality is satisfied.

As an example, we use experimental data from W7-X plasma discharge 20 221 214.028, 2.5–2.9 s, whose magnetic configuration is described in detail in [39]. The Thomson scattering diagnostic was employed for the measurements of n_e and T_e, while T_i was obtained from the the x-ray imaging crystal spectrometer diagnostic. These measured profiles and the corresponding dimensionless plasma parameters are denoted

Table 2. Comparison of global quantities relating to the transition location with their local counterparts in the radially dependent diffusion coefficient model. A comparison of the minima of the electric field derivative is also presented.

Configuration	$r_{\max}$	r_i	r_0	$r^{\zeta}_{\max}$	r^{ζ}_i	r^{ζ}_0	$E'_r(r_i)$	$E'\zeta_r\left(r^{\zeta}_i\right)$
High-mirror	23.7	26.3	27.9	19.2	25.3	25.6	−492.7	−525.1
Low-mirror	18.9	21.1	23.1	14.8	19.0	19.5	−281.1	−297.2
Standard	16.4	18.3	20.6	13.6	18.7	19.2	−332.9	−276.7

with a ~ sign, and a single ion species is assumed, i.e. $\tilde{n} \equiv n_e = n_i$.

Figure 11 shows the results of global simulations and the local radially dependent diffusion coefficient model for this discharge. The agreement of the maxima of the electric field derivatives between the generalised diffusion model and the global simulations confirms the validity of the plateau model for the diffusion coefficient. For this specific case, the transition location for both models agrees well, which may seem surprising in the light of the discussion above. To understand this result, let us first compare the ratio of the dimensionless plasma parameters, $\tilde{\tau}/\tau_{\exp}$, $\tilde{\nu}^i_*/\nu^i_{*,\exp}$, and $\tilde{\rho}^i_*/\rho^i_{*,\exp}$. Figure 12 shows that these ratios are close to unity in most of the plasma. Earlier, it was found that the transition location according to the Maxwell construction coincided with the inflection point of the global simulation for the experimental profiles $T_{i,\exp}$, $T_{e,\exp}$ and $n_{\exp}$ in the W7-X standard configuration (this can be seen in figure 3 for $\alpha = 1$).

Aside from the dependence on the magnetic configuration, the distance between the inflection points of the electric field calculated from the generalised diffusive model and the global simulations is most significantly dependent on the value of the normalised ion gyroradius (figure 10). Since $\tilde{\rho}^i_*$ is smaller than $\rho^i_{*,\exp}$ by approximately 13% throughout most of the plasma, referring to figure 10(*a*), for $\alpha_{\rho^*} = 0.87$ we also expect $r^{\zeta}_i \approx r_i$. Finally, since $r^{\zeta}_i \approx r_*$, we can form a hypothesis that the Maxwell construction gives a reasonable approximation to r_i for W7-X plasmas characterised by a similar density profile to $n_{\exp}$. However, caution should be taken when applying this result, since the dependence of $r_* - r_i$ on the magnetic configuration has not yet been studied in detail, though our results suggest that it is accurately captured by the local models, at least on the qualitative level.

Figure 11(*b*) also shows the threshold for the derivative of the electric field beyond which turbulence is expected to be mitigated. Therefore, based on these results, we can expect that the shear of the $\mathbf{E}\times\mathbf{B}$ flow suppresses the turbulence in a region around the maximum of the derivative of the electric field. In fact, this is the case for all the simulations discussed in this study but it may not always hold. The criterion of equation (54) may not be satisfied, particularly if the electron root is weak. Therefore, for turbulence-related applications, it is essential that the local model accurately predicts the existence of the electron roots and the associated value of the minimum of the electric field, which we have shown to be the case for the radially dependent diffusion coefficient proposed in this article.

8. Conclusions and outlook

We have presented a comparison between the diffusion-equation model for the radial electric field and self-consistent, global neoclassical simulations for the Wendelstein 7-X stellarator. The latter are of course much more rigorous but computationally expensive, and it is therefore of interest to assess how well the diffusion model performs in practice.

In the limit of a small diffusion coefficient, $D \to 0^+$, the diffusion model reduces to the Maxwell construction familiar from thermodynamics, but this is also the case for a broad class of generalisations of this model. For instance, the diffusion coefficient can be taken to depend on radius, or the diffusion operator can be replaced by a self-adjoint higher-order differential operator, or by a linear integral operator with a symmetric kernel. In the appropriate limit, the prediction of all these models reduces to the Maxwell construction as long as the diffusion coefficient, or the generalisation thereof, does not depend on the radial electric field. When compared with global drift-kinetic simulations, the Maxwell construction is however found to be in quantitative disagreement with global indicators of the transition location, such as the zero and the inflection point of the electric field. Furthermore, the transition location calculated with the Maxwell construction does not have the same scaling properties as global indicators when variations in the normalised ion gyroradius are considered (figure 3(*a*)). It does however provide an excellent agreement for the variations with ion collisionality and electron-to-ion temperature ratio. Taking both these facts into account, we can conclude that the agreement of the transition location according to the Maxwell construction with the inflection point of the global electric field (visible in figures 3(*c*) and (*b*)) in these parameterisations seems to be coincidental. Additionally, when the electron-to-ion temperature ratio is small, the Maxwell construction can predict an electron-root solution of the electric field which is not observed in global simulations. On the other hand, spontaneous root transitions with variations in the electron-to-ion temperature ratio, as predicted by the Maxwell construction, have been observed in the global simulations. Within the framework of global theory, it was found that these critical phenomena are likely to be observed close to the magnetic axis, with transitions from ion- to electron-roots at larger

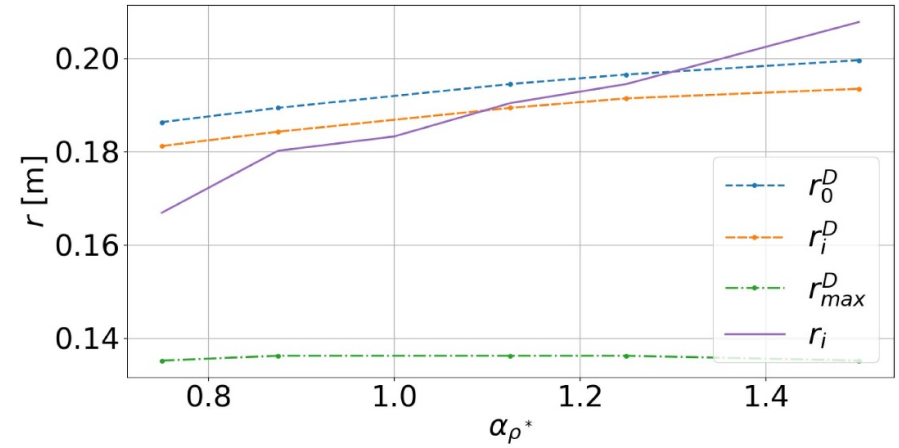

(a) ρ_i^* scaling

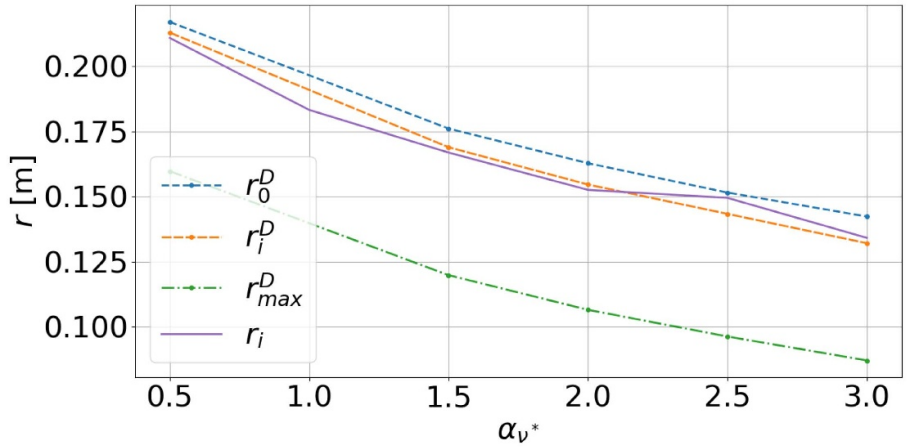

(b) ν_i^* scaling

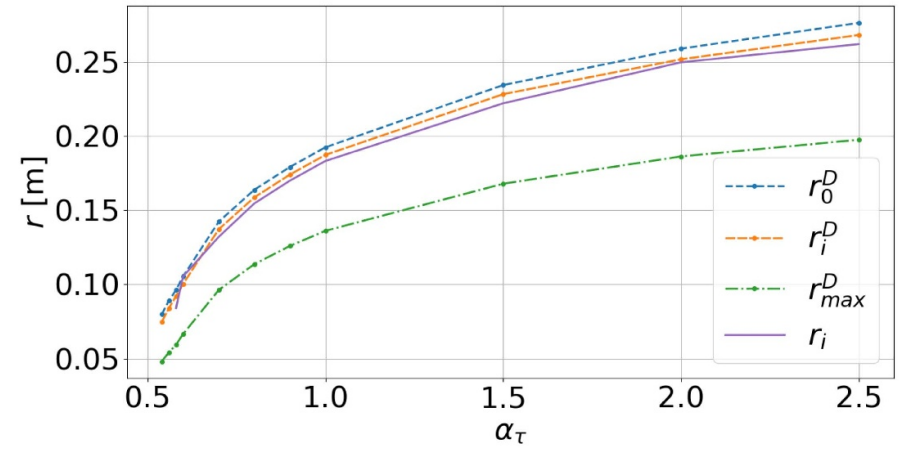

(c) τ scaling

Figure 10. Dependence of r_0^ζ, r_i^ζ, and $r_{\max}^\zeta$ on α for ρ_*^i, ν_*^i and τ parameterisation, for $\zeta = 240.63$ in the proposed diffusion coefficient model. The purple line represents r_i. The positions r_0 and $r_{\max}$ are illustrated in figure 3. Figure 4 shows the corresponding results of the constant diffusion coefficient model.

radii being gradual. For future research, a comparison between the transition location according to the Maxwell construction with global simulations in the small ion gyroradius regime is of importance, since it is potentially relevant for future fusion reactors.

Despite fundamental discrepancies between the predictions of the diffusion model and global kinetic simulations, the former model can be made to perform relatively well if the diffusion coefficient is taken to depend appropriately on the local plasma parameters. A simple recipe has been

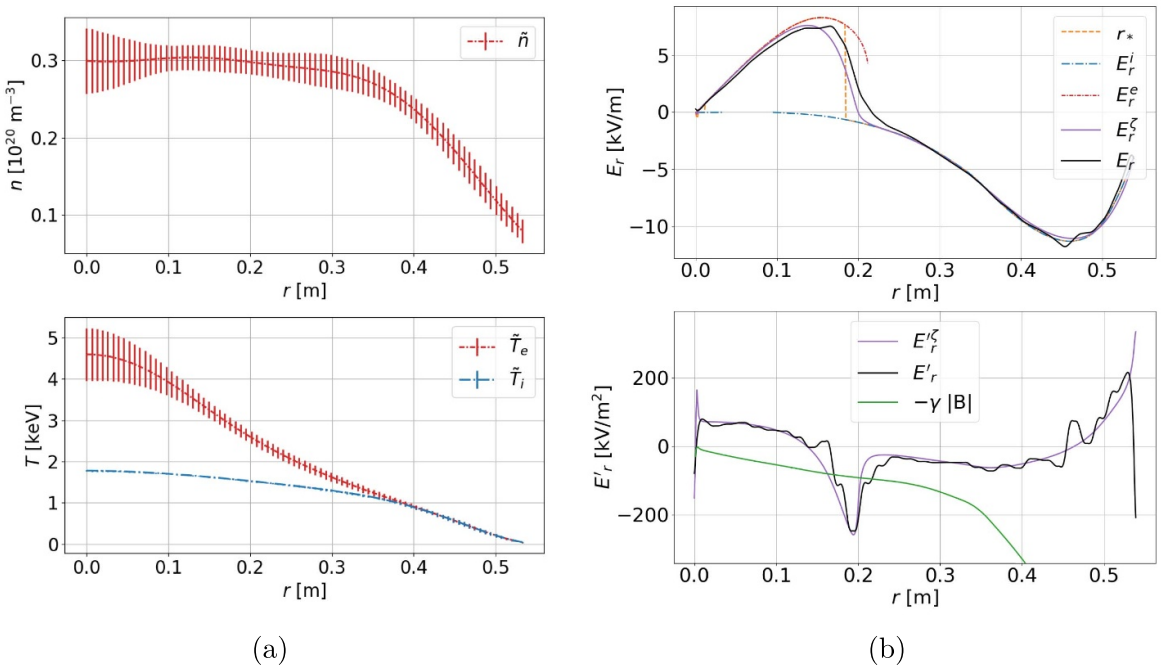

Figure 11. Comparison of electric field and its derivative calculated with global simulations and local radially dependent diffusion coefficient model for testing its predictive capability. The simulated profiles are shown in (*a*), and the electric field and its derivative are depicted in (*b*). The green line depicts the threshold value E_r' for which ITGs are expected to be suppressed. The results consider the FMM002 configuration of W7-X. For the profiles in (*a*), error bars represent three standard deviations.

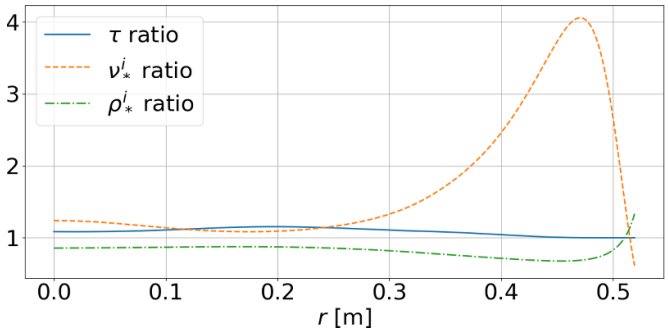

Figure 12. Comparison of $\tilde{\tau}/\tau_{\rm exp}$, $\tilde{\nu}^i_*/\nu^i_{*,\rm exp}$, and $\tilde{\rho}^i_*/\rho^i_{*,\rm exp}$ for the two experimental discharges of W7-X presented in this work. The green line denoted the $\tilde{\rho}^i_*/\rho^i_{*,\rm exp}$ ratio, which is approximately constant and close to unity. Since the ion gyroradius determines $r_i^\zeta - r_i$, we expect this difference to be similar for both experimental discharges.

constructed, $D(r) = \zeta L_{11}^{\rm p}$, where $L_{11}^{\rm p}$ neoclassical particle diffusion coefficient in the plateau regime, and $\zeta \sim 240$, a constant obtained by a fitting procedure. For simulations in the W7-X stellarator, this model correctly accounts for the existence of electron-roots in the low ion-to-electron-temperature-ratio regime. Perhaps most significantly, it replicates the minimum value of the derivative of the global electric field with a considerable degree of precision. Since L_{11}^p is proportional to the square of the gyroradius, the width of the transition layer is inversely proportional to B in the diffusion model. As seen in the gyrokinetic simulations, the layer therefore narrows and the derivative of the electric field becomes large if $\rho_* \to 0$. However this is not necessarily evidence that the electric field indeed satisfies a diffusion equation. The width of the transition layer could, for instance, be set by the orbit width of the trapped-ion trajectories or by the distance a trapped electron or ion drifts radially in a collision time, which would also be inversely proportional to B. A significant drawback of this and simpler local models is that they cannot be used generally to accurately predict the location of the electron-to-ion-root transition. Similarly, as for the case of the Maxwell construction, the agreement of the inflection points calculated with the diffusion models and the global simulations (as seen in figures 4(*b*), (*c*) and 10(*b*), (*c*)) is interpreted to be coincidental. Nevertheless, the overall scaling of the points of interest with ion collisionality and electron-to-ion temperature ratio is reproduced accurately by the diffusion models. However, the diffusion models fail to accurately capture the scaling behaviour with respect to the normalised ion gyroradius (figure 4(*a*) and 10(*a*)).

In the transition region, the radial electric field varies rapidly with radius, leading to a strongly sheared $\mathbf{E} \times \mathbf{B}$ flow, which could locally suppress, or at least reduce, plasma turbulence. If the resulting transport barrier is large enough, overall plasma confinement would improve substantially. As we have seen, the electric field shear can be estimated with the introduced diffusion model, which should be helpful for assessing the possible formation of such transport barriers.

Acknowledgments

This work has been carried out within the framework of the EUROfusion Consortium, funded by the European Union via the Euratom Research and Training Programme (Grant Agreement No. 101052200—EUROfusion). Views and opinions expressed are however those of the author(s) only and do not necessarily reflect those of the European Union or the European Commission. Neither the European Union nor the European Commission can be held responsible for them.

Appendix. Formulation of the electric-field diffusion equation using Prigogine's theorem

The electric-field diffusion equation can be derived by applying Prigogine's theorem to the neoclassical transport theory of non-axisymmetric stellarators. This approach aligns with the historical development of the neoclassical theory and will be discussed subsequently.

Prigogine's theorem states that a thermodynamic system evolves in such a way that the entropy production rate is at a minimum in the stationary state. A sufficient condition for this theorem to hold is that the Onsager matrix of transport coefficients, which relates the generalised forces to fluxes, is a constant matrix. However, the requirement that the relationship between thermodynamic forces and the resulting neoclassical fluxes be linear is violated for neoclassical transport [16]. For instance, considering the 'pure' $\sqrt{\nu}$ low-collisionality transport regime, it is apparent that the mono-energetic diffusion coefficient D_{11} scales as $|E_r|^{-3/2}$, making L_{11} dependent on E_r. Thus, for neoclassical transport, the Prigogine's theorem may, at best, only be treated as an approximate tool [17]. With this assumption, the entropy production rate is given by

$$\dot{S}[E_r] = \int_0^a \left\{ \frac{e}{\epsilon} \int^{E_r} (Z_i\Gamma_i - \Gamma_e)\, \mathrm{d}E_r' \right\} V' \mathrm{d}r. \tag{55}$$

This functional has a local minimum when E_r is equal to either E_r^i or E_r^e. The global minimum is obtained at every radius by choosing E_r as the root that gives the lowest value of the integral in the brackets. This immediately implies the Maxwell construction.

If D is independent on E_r, equation (55) can be generalised as follows [29],

$$\dot{S} = \int_0^a \left\{ \frac{D}{2} \left(E_r' - \frac{E_r}{r} \right)^2 + \frac{e}{\epsilon} \int (Z_i\Gamma_i - \Gamma_e)\, \mathrm{d}E_r \right\} V' \mathrm{d}r, \tag{56}$$

where the first term models the heat production rate, ensuring that its contribution vanishes for rotation with constant angular frequency ($E_r \propto r$) [40]. Solving the Euler–Lagrange equations for equation (56) results in

$$-\frac{1}{V'r}\frac{\partial}{\partial r} DV' r^2 \frac{\partial}{\partial r}\frac{E_r}{r} = \frac{e}{\epsilon}(\Gamma_e - Z_i\Gamma_i). \tag{57}$$

It is apparent that this equation differs from the stationary-state of equation (17). However, in this work we, decided to study equation (17), since this is the equation implemented in the code NTSS [29], which is a popular tool for the analysis of neoclassical transport in stellarators. It should be noted that the choice between equations (17) and (57) is to some extent arbitrary, since in either case, they merely attempt to model the nonlocal effects by introducing a diffusive term not derived from first principles.

Finally, we remark that the Maxwell construction still applies to equation (57), since by choosing $f(r) = -1/rV'$, $g(r) = V'r^2$, and $h(r) = 1/r$, it can be written in the form of equation (26). Should there be a discrepancy between the transition location derived from the Maxwell construction and that obtained from global simulations in the limit $\rho_* \to 0$, it would indicate (unsurprisingly) that Prigogine's theorem does not hold for neoclassical transport in stellarators.

ORCID iDs

M.D. Kuczyński https://orcid.org/0000-0001-8595-9816
R. Kleiber https://orcid.org/0000-0002-2261-2855
P. Helander https://orcid.org/0000-0002-0460-590X
S. Bozhenkov https://orcid.org/0000-0003-4289-3532
A. Langenberg https://orcid.org/0000-0002-2107-5488
T. Andreeva https://orcid.org/0000-0003-2390-4240

References

[1] Maurer M., Bañón Navarro A., Dannert T., Restelli M., Hindenlang F., Görler T., Told D., Jarema D., Merlo G. and Jenko F. 2020 GENE-3D: a global gyrokinetic turbulence code for stellarators *J. Comput. Phys.* **420** 109694
[2] Satake S., Kanno R. and Sugama H. 2008 Development of a non-local neoclassical transport code for helical configurations *Plasma Fusion Res.* **3** S1062
[3] Kleiber R. *et al* 2024 EUTERPE: a global gyrokinetic code for stellarator geometry *Comput. Phys. Commun.* **295** 109013
[4] Helander P., Bird T., Jenko F., Kleiber R., Plunk G.G., Proll J.H.E., Riemann J. and Xanthopoulos P. 2015 Advances in stellarator gyrokinetics *Nucl. Fusion* **55** 053030
[5] Sánchez E. *et al* 2021 Gyrokinetic simulations in stellarators using different computational domains *Nucl. Fusion* **61** 116074
[6] Beidler C.D. *et al* 2021 Demonstration of reduced neoclassical energy transport in Wendelstein 7-X *Nature* **596** 221–6
[7] Tribaldos V. and Guasp J. 2005 Neoclassical global flux simulations in stellarators *Plasma Phys. Control. Fusion* **47** 545
[8] Yokoyama M. *et al* 2007 Core electron-root confinement (CERC) in helical plasmas *Nucl. Fusion* **47** 1213
[9] Sun Y., Shaing K.C., Liang Y., Casper T., Loarte A., Shen B. and Wan B. 2013 Intrinsic plasma rotation determined by neoclassical toroidal plasma viscosity in tokamaks *Nucl. Fusion* **53** 093010
[10] Li H., Sun Y., Wang L., He K. and Shaing K.-C. 2021 Symmetry breaking driving spontaneous plasma rotation in tokamak fusion devices *Nucl. Fusion* **61** 104002
[11] Beidler C.D., Drevlak M., Geiger J., Helander P., Smith H.M. and Turkin Y. 2024 Reduction of neoclassical bulk-ion transport to avoid helium-ash retention in stellarator reactors *Nucl. Fusion* **64** 126030

[12] Terry P.W. 2000 Suppression of turbulence and transport by sheared flow *Rev. Mod. Phys.* **72** 109–65
[13] Shaing K.C. 1984 Stability of the radial electric field in a nonaxisymmetric torus *Phys. Fluids* **27** 1567–9
[14] Shaing K.C. 1984 Noise-induced transition of the radial electric field in a nonaxisymmetric torus *Phys. Fluids* **27** 1924–6
[15] Catto P.J. and Myra J.R. 1986 Comments on "Stability of the radial electric field in a nonaxisymmetric torus" [Phys. Fluids 27, 1567 (1984)] *Phys. Fluids* **29** 2020
[16] Hastings D.E. 1986 Bifurcation phenomena and the radial electric field in a nonaxisymmetric plasma *Phys. Fluids* **29** 536–43
[17] Catto P.J., Myra J.R. and Hastings D.E. 1986 Comments on "Bifurcation phenomena and the radial electric field in a nonaxisymmetric plasma" [Phys. Fluids 29, 536 (1986)] *Phys. Fluids* **29** 2760–1
[18] Dinklage A. *et al* 2018 Magnetic configuration effects on the Wendelstein 7-X stellarator *Nat. Phys.* **14** 855–60
[19] Kuczyński M.D., Kleiber R., Smith H.M., Beidler C.D., Borchardt M., Geiger J. and Helander P. 2024 Self-consistent, global, neoclassical radial-electric-field calculations of electron-ion-root transitions in the W7-X stellarator *Nucl. Fusion* **64** 046023
[20] Beidler C.D. *et al* 2011 Benchmarking of the mono-energetic transport coefficients—results from the International Collaboration on Neoclassical Transport in Stellarators (ICNTS) *Nucl. Fusion* **51** 076001
[21] Helander P. and Sigmar D.J. 2002 *Collisional Transport in Magnetized Plasmas* (Cambridge University Press)
[22] Hirshman S.P., Shaing K.C., van Rij W.I., Beasley J.C.O. and Crume J.E.C. 1986 Plasma transport coefficients for nonsymmetric toroidal confinement systems *Phys. Fluids* **29** 2951–9
[23] van Rij W.I. and Hirshman S.P. 1989 Variational bounds for transport coefficients in three-dimensional toroidal plasmas *Phys. Fluids* B **1** 563–9
[24] Helander P. and Simakov A.N. 2008 Intrinsic ambipolarity and rotation in stellarators *Phys. Rev. Lett.* **101** 145003
[25] Calvo I., Parra F.I., Velasco J.L. and Alonso J.A. 2013 Stellarators close to quasisymmetry *Plasma Phys. Control. Fusion* **55** 125014
[26] Helander P. 2014 Theory of plasma confinement in non-axisymmetric magnetic fields *Rep. Prog. Phys.* **77** 087001
[27] Pablant N. *et al* 2018 Dependence of the core radial electric field on ion and electron temperature in W7-X *45th EPS Conf. on Plasma Physics* (European Physical Society) p P2.1102
[28] Hastings D.E., Houlberg W.A. and Shaing K.C. 1985 The ambipolar electric field in stellarators *Nucl. Fusion* **25** 445
[29] Turkin Y., Beidler C.D., Maaßberg H., Murakami S., Tribaldos V. and Wakasa A. 2011 Neoclassical transport simulations for stellarators *Phys. Plasmas* **18** 022505
[30] Kleiber R., Hatzky R., Könies A., Kauffmann K. and Helander P. 2011 An improved control-variate scheme for particle-in-cell simulations with collisions *Comput. Phys. Commun.* **182** 1005–12
[31] Neuner U. *et al* 2021 Measurements of the parameter dependencies of the bootstrap current in the W7-X stellarator *Nucl. Fusion* **61** 036024
[32] Geiger J., Beidler C.D., Feng Y., Maaßberg H., Marushchenko N.B. and Turkin Y. 2014 Physics in the magnetic configuration space of W7-X *Plasma Phys. Control. Fusion* **57** 014004
[33] Connor J.W. and Taylor J.B. 1977 Scaling laws for plasma confinement *Nucl. Fusion* **17** 1047
[34] Helander P. and Plunk G.G. 2022 Energetic bounds on gyrokinetic instabilities. Part 1. Fundamentals *J. Plasma Phys.* **88** 905880207
[35] Zocco A., Podavini L., Garcìa-Regaña J.M., Barnes M., Parra F.I., Mishchenko A. and Helander P. 2022 Gyrokinetic electrostatic turbulence close to marginality in the Wendelstein 7-X stellarator *Phys. Rev.* E **106** L013202
[36] Bähner J.-P. *et al* 2021 Phase contrast imaging measurements and numerical simulations of turbulent density fluctuations in gas-fuelled ECRH discharges in Wendelstein 7-X *J. Plasma Phys.* **87** 905870314
[37] Waltz R.E., Kerbel G.D. and Milovich J. 1994 Toroidal gyro-Landau fluid model turbulence simulations in a nonlinear ballooning mode representation with radial modes *Phys. Plasmas* **1** 2229–44
[38] Ivanov P.G.I., Adkins T., Kennedy D., Giacomin M., Barnes M. and Schekochihin A.A. 2024 Suppression of temperature-gradient-driven turbulence by sheared flows in fusion plasmas (arXiv:2405.00854)
[39] Andreeva T. *et al* 2022 Magnetic configuration scans during divertor operation of Wendelstein 7-X *Nucl. Fusion* **62** 026032
[40] Maassberg H., Burhenn R., Gasparino U., Kühner G., Ringler H. and Dyabilin K.S. 1993 Experimental and neoclassical electron heat transport in the LMFP regime for the stellarators W7-A, L-2 and W7-AS *Phys. Fluids* B **5** 3627–40